

1 **A Conceptual Model of Polar Overturning Circulations**

2 Thomas W. N. Haine*

3 *Earth & Planetary Sciences, Johns Hopkins University, Baltimore, Maryland*

4 *Corresponding author: Thomas W. N. Haine, Thomas.Haine@jhu.edu

ABSTRACT

5 The global ocean overturning circulation carries warm, salty water to high latitudes, both
6 in the Arctic and Antarctic. Interaction with the atmosphere transforms this inflow into three
7 distinct products: sea ice, surface Polar Water, and deep Overflow Water. The Polar Water and
8 Overflow Water form estuarine and thermal overturning cells, stratified by salinity and temperature,
9 respectively. A conceptual model specifies the characteristics of these water masses and cells given
10 the inflow and air/sea/land fluxes of heat and freshwater. The model includes budgets of mass,
11 salt, and heat, and parametrizations of Polar Water and Overflow Water formation, which include
12 exchange with continental shelves. Model solutions are mainly controlled by a linear combination
13 of air/sea/ice heat and freshwater fluxes and inflow heat flux. The model shows that for the Arctic,
14 the thermal overturning is likely robust, but the estuarine cell appears vulnerable to collapse via a
15 so-called heat crisis that violates the budget equations. The system is pushed towards this crisis by
16 increasing Atlantic Water inflow heat flux, increasing meteoric freshwater flux, and/or decreasing
17 heat loss to the atmosphere. The Antarctic appears close to a so-called Overflow Water emergency
18 with weak constraints on the strengths of the estuarine and thermal cells, uncertain sensitivity to
19 parameters, and possibility of collapse of the thermal cell.

20 **1. Introduction**

21 The global ocean overturning circulation is transformed in the high latitudes of both hemispheres.
22 The transformation is achieved by extraction of heat to the atmosphere, addition of meteoric
23 freshwater, and interaction with ice. Understanding how warm salty inflows to polar oceans
24 partition into different outflow components is primitive, however, and this question is important
25 for oceanography and climate science. To address it, this paper presents and explores a conceptual
26 physical model and applies it to both the Arctic and the Antarctic.

27 The Arctic Ocean and Nordic Seas are separated from the global ocean by relatively shallow
28 ridges between Greenland and Scotland. The flow across these ridges consists of surface-intensified
29 warm salty water from the North Atlantic Current flowing north (Hansen et al. 2008). Returning
30 south are three distinct water types (Hansen and Østerhus 2000; Østerhus et al. 2005). First, there
31 is overflow water, which spills into the North Atlantic Ocean through gaps in the ridges. Overflow
32 water is cooler and denser than the inflow, but of similar salinity. Second, there is a cold fresh
33 surface outflow in the East Greenland Current (Rudels et al. 2002). The East Greenland Current
34 also carries the third water type, which is sea ice.

35 The exchange between the Nordic Seas and the Arctic Ocean across the Fram Strait and Barents
36 Sea Opening is essentially the same. Fig. 1 shows the hydrographic characteristics and currents.
37 The warm salty inflow is Atlantic Water (AW), which flows north in the eastern halves of the Barents
38 Sea Opening and the Fram Strait. The net AW flux into the Arctic is about 4 Sv (Tsubouchi et al.
39 2012, 2018; some also recirculates in Fram Strait; 1 Sv equals $10^6 \text{m}^3 \text{s}^{-1}$). The AW temperature
40 exceeds about 3°C with a salinity around 35.00 g/kg and a seasonal cycle that leads to summer
41 surface freshening and warming (Fig. 1 lower panel). The three outflows are Overflow Water
42 (OW), which is cooler and denser than AW, but of similar salinity (the closest water type from

43 Tsubouchi et al. (2018) is their Intermediate Water, but we adopt OW here, consistent with Eldevik
44 and Nilsen 2013). OW leaves the Arctic on the western side of Fram Strait in the deep part of the
45 East Greenland Current. Above OW is Polar Water (PW), which is near the freezing temperature
46 and fresher than AW (Tsubouchi et al. 2018 call this Surface Water). As for AW, the PW is warmer
47 and fresher in summer. Sea ice occupies the western part of Fram Strait and the East Greenland
48 continental shelf, flowing in the East Greenland Current. The split between OW and PW transport
49 is about 3:1 (this estimate, from Tsubouchi et al. 2018 Fig. 4, is representative not precise, due
50 mainly to the non-zero flow across Fram Strait and the Barents Sea Opening). The sea ice flux is
51 about 0.064 Sv (Haine et al. 2015).

52 The Antarctic overturning circulation is essentially similar. The inflow of warm salty water
53 occurs in Circumpolar Deep Water (CDW), analogous to AW (it is called AW below), and fed
54 from the North Atlantic overflows. CDW upwells towards the surface beneath the Antarctic
55 Circumpolar Current (Marshall and Speer 2012; Talley 2013). Air/sea/ice interaction around
56 Antarctica transforms the CDW in two meridional overturning cells that circulate back north. The
57 stronger cell is the upper one with a transport of about 22 Sv, equivalent to 80% of the CDW
58 flux (Abernathey et al. 2016; Pellichero et al. 2018). This cell feeds fresh, cold surface water
59 that is called Winter Water when the summer thermal stratification is removed. It is analogous
60 to Arctic PW. The Winter Water flows north and subducts as Subantarctic Mode Water (SAMW)
61 and Antarctic Intermediate Water (AAIW), which are less dense than CDW mainly because they
62 are fresher. Associated with Winter Water is sea ice, which forms primarily near Antarctica in
63 winter and flows north with a flux of about 0.36 Sv (Abernathey et al. 2016). The weaker, lower
64 cell produces Antarctic Bottom Water (AABW) from CDW by cooling and salinification. AABW
65 is analogous to Arctic OW. It forms from CDW by freezing and brine rejection, especially on the
66 continental shelves in the Weddell and Ross Seas and around east Antarctica (Foster and Carmack

67 1976; Orsi et al. 1999; Jacobs 2004). The resulting dense, saline, freezing shelf water overflows the
68 shelf break into the deep ocean. As it descends, the dense plume entrains and mixes with ambient
69 CDW to form AABW (Muench et al. 2009; Naveira Garabato et al. 2002).

70 To our knowledge, no prior study quantifies both estuarine and thermal overturning cells in the
71 Arctic and Antarctic. Nevertheless, the key ideas in the present model are well known in the polar
72 oceanography literature. First, consider the salinization process to produce dense shelf water: Gill
73 (1973) argues that brine release during winter freezing on the continental shelves of the Weddell
74 Sea produces dense saline water that overflows the shelf break to form AABW. He points to the wind
75 driven export of sea ice offshore to maintain high freezing rates in coastal polynyas. This process is
76 corroborated using satellite microwave data in the Arctic by Tamura and Ohshima (2011). Aagaard
77 et al. (1981) describe the maintenance of the Arctic halocline by salinization of shelf water in winter
78 by freezing and export of sea ice. Their observations show freezing shelf water with high salinity,
79 in some cases 2–4 g/kg higher than in summer. Extending this work, Aagaard et al. (1985) propose
80 that a major source of Arctic deep water is dense brine-enriched shelf water. Quadfasel et al.
81 (1988) present observational evidence of the shelf overflow and entrainment process occurring in
82 Storfjorden, Svalbard. They observe shelf water with salinities of about 35.5 g/kg (about 0.5 g/kg
83 saltier than the AW in Fram Strait) at the freezing temperature (see also Maus 2003). Rudels and
84 Quadfasel (1991) review the importance of dense shelf water overflow to the maintenance of the
85 deep Arctic Ocean thermohaline structure. They conclude that it must dominate open-ocean deep
86 convection, although this latter process occurs variably in the Greenland Sea. Freezing and brine
87 rejection drive both deep convection and shelf overflows in their view, consistent with Aagaard
88 et al. (1985).

89 More recently, Rudels (2010, 2012) articulates the problem of understanding Arctic water mass
90 transformation and the Arctic estuarine and thermal overturning cells together (he refers to them as

91 a “double estuary”). His papers address several issues that underpin the present work: formation
92 of the fresh PW layer, conversion of AW to PW, separation between the estuarine and thermal cells,
93 formation of deep water, and exchange through Fram Strait. Abernathey et al. (2016) and Pellichero
94 et al. (2018) also view the Antarctic system in an holistic way. They focus on the upper estuarine
95 cell and the importance of sea ice in fluxing freshwater from the shelves to freshen SAMW and
96 AAIW. Eldevik and Nilsen (2013) define the problem of quantifying the two Arctic overturning
97 cells (they refer to them as the “Arctic-Atlantic thermohaline circulation”). Their model consists
98 of volume, salinity, and heat budgets, similar to eq. (1) below. However, to close their problem and
99 solve for the outflow transports they must specify the temperature and salinity properties of PW
100 and OW. They also neglect sea ice. Therefore, their system is a special case of the model presented
101 here, which does not make these assumptions.

102 This paper synthesizes the ideas outlined above. It builds, explains, and applies a quantitative
103 model of polar overturning circulation. The model is conceptual so as to elucidate principles and
104 characteristics. It neglects many important effects including seasonality, interannual variability,
105 regional differences, and continuously varying hydrographic properties. It includes budgets for
106 mass, salt, and heat and physical parametrizations of PW and OW formation. Although it re-
107 spects physical principles, the model is essentially kinematic. The dynamics of the overturning
108 circulations are beyond the model’s scope, and likely differ between the Arctic and Antarctic.
109 Nevertheless, the dynamics must in aggregate respect the budget and parametrization equations
110 used here.

111 **2. Conceptual Model**

112 Consider the system sketched in Fig. 2: A deep polar basin is fed across a gateway from lower
113 latitudes with relatively warm, salty Atlantic Water (AW). The polar basin connects to a shallow

114 polar continental shelf across a shelf break. The basin and shelf exchange heat and freshwater with
 115 the atmosphere. The basin returns three distinct water classes to lower latitudes (see Fig. 3 for a
 116 temperature/salinity schematic), namely: Overflow Water (OW), which is a cooled, denser version
 117 of AW, with similar salinity; Polar Water (PW), which is a fresh, freezing, less dense version of
 118 AW; and, sea ice. Sea ice formation (freezing) occurs on the shelf and there is partial sea ice
 119 melting in the basin. The AW to OW pathway comprises the thermal overturning cell and the AW
 120 to PW plus sea ice comprises the estuarine overturning cell.

121 The model specifies steady seawater mass, heat, and salt mass budgets for two control volumes:
 122 the basin melting region and the continental shelf freezing region (see also Eldevik and Nilsen
 123 2013). In the **basin** (region A):

$$\begin{aligned}
 & \rho_1 U_1 + \rho_2 U_2 + \rho_3 U_3 + \rho_i U_i - \rho_1 u_1 - \rho_i u_i - \rho_s u_s = \mathcal{F}_b, \\
 & \rho_1 U_1 S_1 + \rho_2 U_2 S_2 + \rho_3 U_3 S_3 + \rho_i U_i S_i - \rho_1 u_1 S_1 - \rho_i u_i S_i - \rho_s u_s S_s = 0, \\
 & c_p (\rho_1 U_1 T_1 + \rho_2 U_2 T_2 + \rho_3 U_3 T_3 - \rho_1 T_1 u_1 - \rho_s T_s u_s) - \rho_i L' (U_i - u_i) = Q_b. \quad (1)
 \end{aligned}$$

124 Full details on notation are in Table 1. The volume fluxes (transports) are U_j , temperatures are T_j ,
 125 and salinities are S_j (the associated density is $\rho_j = \rho(T_j, S_j)$). The j subscripts correspond to: 1 =
 126 Atlantic Water (AW), 2 = Polar Water (PW), 3 = Overflow Water (OW). The AW flux parameters
 127 $U_1, U_1 T_1$ and $U_1 S_1$ are provided. The surface ocean freshwater mass and heat flux parameters are
 128 \mathcal{F}_b ¹ and Q_b , respectively. The sign conventions are:

- 129 • Positive volume fluxes U_j mean poleward flow. So U_1 is positive and all the others are negative.
- 130 • Positive fluxes \mathcal{F}_b, Q_b mean ocean to atmosphere freshwater and heat fluxes (i.e., ocean
 131 salinifying and cooling). So \mathcal{F}_b is negative and Q_b is positive.

¹Inflowing freshwater is assumed to have a temperature of 0°C.

132 Assume that not all the sea ice melts, $U_i \leq 0$, and therefore

$$T_2 = T_f, \quad (2)$$

133 where T_f is the freezing temperature (evaluated at the appropriate salinity, which is S_2 here).

134 Finally, $L' = L - c_p T_f + c_i (T_f - T_i)$, L is the latent heat of freezing for seawater, T_i is sea ice
135 temperature, and c_p, c_i are the specific heat capacities of seawater and sea ice, respectively.

136 Similarly, on the **shelf** (region B):

$$\begin{aligned} \rho_1 u_1 + \rho_s u_s + \rho_i u_i &= \mathcal{F}_s, \\ \rho_1 S_1 u_1 + \rho_s S_s u_s + \rho_i S_i u_i &= 0, \\ c_p (\rho_1 T_1 u_1 + \rho_s T_f u_s) - \rho_i L' u_i &= \mathcal{Q}_s, \end{aligned} \quad (3)$$

137 where the lower case u 's indicate the shelf break fluxes and the subscript s indicates Shelf Water
138 (SW) properties. Assume that SW forms from AW by cooling and freshwater input (with no PW
139 contribution). The products are SW with properties T_s, S_s and sea ice that leaves the shelf for the
140 basin. Freezing requires that $u_i \leq 0$ and therefore

$$T_s = T_f. \quad (4)$$

141 Assume that PW is formed from AW by heat loss to the atmosphere and to melt sea ice, following
142 Klinger and Haine (2019) Chapter 10. See also Rudels (2016), references therein, Abernathey et al.
143 (2016); Pellichero et al. (2018) and Fig. 3. The AW is cooled to freezing temperature and freshened
144 by melt. In order to maintain the stably stratified PW layer above the AW layer, we require that
145 $\rho_2 \leq \rho_1$. This sets the maximum allowed PW salinity given the AW inflow properties:

$$S_2 \leq \frac{\beta (S_1 - S_i) (L' + c_p T_f) S_1 + \alpha (T_1 - T_f) (L' + c_p T_1) S_i}{\beta (S_1 - S_i) (L' + c_p T_f) + \alpha (T_1 - T_f) (L' + c_p T_1)}, \quad (5)$$

146 where α and β are the thermal expansion and haline contraction coefficients (evaluated at the AW
147 temperature and salinity).

148 Assume that OW is formed from SW and a mixture of AW and PW that is entrained during the
 149 overflow. The Price and O'Neil Baringer (1994) model is used for this process (their end-point
 150 model, not the streamtube model: see also discussion in section 4). It computes the product
 151 properties of the plume of OW descending from a marginal sea and entraining ambient water (aW).
 152 Consider two cases:

- 153 • Entraining case for $F_{\text{geo}} \geq 1, \Phi > 0$:

$$\begin{aligned}
 T_3 &= \Phi T_a + (1 - \Phi) T_s, \\
 S_3 &= \Phi S_a + (1 - \Phi) S_s,
 \end{aligned}
 \tag{6}$$

154 where $(T_s = T_f, S_s)$ are the SW properties, (T_a, S_a) are the aW properties (i.e., the water that
 155 is entrained), and the entrainment parameter $0 \leq \Phi \leq 1$ is

$$\Phi = 1 - F_{\text{geo}}^{-2/3}
 \tag{7}$$

156 for geostrophic Froude number

$$F_{\text{geo}} = \frac{g (\rho_s - \rho_a) \alpha_{\text{max}}^{3/2} (W_s + 2K_{\text{geo}}x)^{1/2}}{\rho_0 f^{3/2} u_s^{1/2}}.
 \tag{8}$$

157 The parameters in (8) are: g gravitational acceleration, ρ_0 seawater reference density, α_{max}
 158 maximum bathymetric slope (not thermal expansion coefficient), f Coriolis parameter, K_{geo}
 159 the geostrophic Ekman number, x the distance downstream from the shelf break, W_s the initial
 160 plume width at the shelf, and u_s the initial plume volume flux leaving the shelf. In deriving
 161 (8), Price and O'Neil Baringer (1994) assume the plume is geostrophic and the bottom stress
 162 causes the plume to grow downstream in width.

163 • Non-entraining case for $F_{\text{geo}} \leq 1, \Phi = 0$ (see also section 4):

$$\begin{aligned} T_3 &= T_s, \\ S_3 &= S_s. \end{aligned} \tag{9}$$

164 Whether or not entrainment occurs, this overflow model prescribes two more equations to compute
165 the OW properties, (T_3, S_3) .

166 Additional assumptions are:

167 1. The aW properties (entrained in the plume) are set by a mixture, $0 \leq \phi \leq 1$, between surface
168 PW and AW:

$$\begin{aligned} T_a &= \phi T_f + (1 - \phi) T_1, \\ S_a &= \phi S_2 + (1 - \phi) S_1. \end{aligned} \tag{10}$$

169 The mixture fraction ϕ is formally another parameter in the conceptual model. It is constrained,
170 however, and it is initially held fixed. Section 3g discusses this assumption.

171 2. The volume flux of OW leaving the system equals the flux after entrainment ceases:

$$U_3 = \frac{u_s}{1 - \Phi}. \tag{11}$$

172 This last equation is another constraint on the system.

173 *a. Conceptual Model Equations*

174 The full system is therefore:

$$\begin{aligned}
 \rho_1 U_1 + \rho_2 U_2 + \rho_3 U_3 + \rho_i U_i - \rho_1 u_1 - \rho_s u_s - \rho_i u_i &= \mathcal{F}_b, \\
 \rho_1 U_1 S_1 + \rho_2 U_2 S_2 + \rho_3 U_3 S_3 + \rho_i U_i S_i - \rho_1 u_1 S_1 - \rho_s u_s S_s - \rho_i u_i S_i &= 0, \\
 c_p (\rho_1 U_1 T_1 + \rho_2 U_2 T_f + \rho_3 U_3 T_3 - \rho_1 u_1 T_1 - \rho_s u_s T_f) - \rho_i L' (U_i - u_i) &= \mathcal{Q}_b, \\
 \rho_1 u_1 + \rho_s u_s + \rho_i u_i &= \mathcal{F}_s, \\
 \rho_1 u_1 S_1 + \rho_s u_s S_s + \rho_i u_i S_i &= 0, \\
 c_p (\rho_1 u_1 T_1 + \rho_s u_s T_f) - \rho_i L' u_i &= \mathcal{Q}_s, \tag{12}
 \end{aligned}$$

175 with intermediate variables:

$$T_a = \phi T_f + (1 - \phi) T_1, \tag{13}$$

$$S_a = \phi S_2 + (1 - \phi) S_1, \tag{14}$$

$$\rho_a = \rho(T_a, S_a), \tag{15}$$

$$\rho_2 = \rho(T_f, S_2)$$

$$\rho_s = \rho(T_f, S_s) \tag{16}$$

$$\Phi = 1 - \gamma \frac{|u_s|^{1/3}}{(\rho_s - \rho_a)^{2/3}}, \tag{17}$$

$$T_3 = \Phi T_a + (1 - \Phi) T_f, \tag{18}$$

$$S_3 = \Phi S_a + (1 - \Phi) S_s, \tag{19}$$

$$\rho_3 = \rho(T_3, S_3), \tag{20}$$

$$u_s = (1 - \Phi) U_3, \tag{21}$$

176 $\gamma = \rho_0^{2/3} f g^{-2/3} \alpha_{\max}^{-1} (W_s + 2K_{\text{geo}x})^{-1/3}$ (see section 3j), and $L' = L - c_p T_f + c_i (T_f - T_i)$. The
 177 inequalities are:

$$S_2 \leq \frac{\beta (S_1 - S_i) (L' + c_p T_f) S_1 + \alpha (T_1 - T_f) (L' + c_p T_1) S_i}{\beta (S_1 - S_i) (L' + c_p T_f) + \alpha (T_1 - T_f) (L' + c_p T_1)}, \quad (22)$$

$$u_i < U_i < 0, \quad (23)$$

$$U_2, U_3, u_s < 0, \quad (24)$$

$$u_1 > 0, \quad (25)$$

$$\rho(T_f, S_s) \geq \rho(T_3, S_3) \geq \rho(T_1, S_1), \quad (26)$$

$$0 \leq \{\Phi, \phi\} \leq 1. \quad (27)$$

178 This is a system of six equations in six unknowns, namely, $\{U_2, U_3, U_i, u_1, u_i, S_s\}$, with
 179 intermediate variables $\{\rho_2, \rho_3, \rho_s, \rho_a, T_3, T_a, S_3, S_a, u_s, \Phi\}$. There are five flux parameters:
 180 $\{U_1, U_1 T_1, U_1 S_1, Q = Q_b + Q_s, \mathcal{F} = \mathcal{F}_b + \mathcal{F}_s\}$, with intermediate parameter $\rho_1 = \rho(T_1, S_1)$, and the
 181 overflow mixing fraction ϕ .

182 *b. Numerical Solution*

183 The model consists of coupled nonlinear algebraic equations. The most important nonlinearity
 184 is due to the parametrization of entrainment (17) and (21), although there are several others due to
 185 the advective product of variables, like $T_3 U_3$, and seawater functions of state, like $\rho_3 = \rho(T_3, S_3)$.
 186 Therefore, the system is solved numerically using a procedure explained in supplement section
 187 S1. Numerical solutions satisfy the equations exactly except for (17), which is satisfied within a
 188 tolerance $\delta\Phi$ because this is likely the most uncertain part of the model. For a given parameter
 189 set, there are typically zero or an infinite number of solutions. The infinite number of solutions is
 190 bounded within limits, which are typically tight.

3. Results

a. Arctic Reference Solutions and Sensitivity to Q

Fig. 4 shows results from experiment 1 using parameters roughly appropriate to the Fram Strait and Barents Sea Opening. The parameters (Table 2) are $U_1 = 4.75$ Sv, $T_1 = 3.4^\circ\text{C}$, $S_1 = 35.00$ g/kg, $Q = 115$ TW, and $\mathcal{F} = -180 \times 10^6$ kgs⁻¹, which are taken from Tsubouchi et al. (2012) and Tsubouchi et al. (2018). The temperature/salinity diagram in Fig. 4 shows the properties of the various water masses. The OW properties T_3, S_3 range over different values, which correspond to a range of SW salinities S_s . Notice that the OW and PW properties are moderately realistic compared to the data shown in Fig. 1. The SW salinities are high, however, and the OW properties cluster close to the aW (indicated by the blue cross). This fact indicates that the entrainment is high for this solution, and indeed, $\Phi = 0.94$. Therefore, the shelf circulation is relatively weak and most OW is formed by AW being entrained into the overflowing SW. Hence, the OW temperature T_3 is relatively high. In this experiment the system balances the heat budget by exporting warm OW. Indeed, experiment 1 has a strong thermal overturning cell compared to the estuarine cell, $U_3/U_2 \approx 3.4$. This ratio is moderately realistic compared to the data shown in Fig. 1 (section 1). The ice export flux, $|U_i|/U_1 \approx 0.040$, is also moderately realistic.

Notice the blue error bars in Fig. 4. They indicate the full range of possible solutions for the fixed parameters in experiment 1 (namely, the 0 and 100 percentiles). The bars themselves indicate the solution with entrainment closest to the mean entrainment (other choices are possible). There are two reasons that a range of solutions exists (see supplement section S1). First, for the fluxes in and out of the system as a whole (across section A; left column in Fig. 4), multiple solutions exist for $\{U_2, U_3, U_i, S_s\}$, and hence $\{u_s, T_3, S_3, \Phi\}$. This multiplicity reflects a tradeoff between shelf salinity S_s and entrainment Φ and is discussed below in section 3c. Second, for the fluxes across the shelf

214 break (across section B; right column in Fig. 4), multiple solutions exist for u_1 and u_i (in principle,
215 for every value of S_s ; the bars show the mean values). This multiplicity reflects a tradeoff between
216 the ocean surface fluxes Q_s and \mathcal{F}_s on the shelf (it is a linear relation, see (S5)). Physically, this
217 second tradeoff means that the shelf heat budget can be satisfied with relatively large Q_s (which is
218 positive), large u_i , large \mathcal{F}_s (negative), and small u_s ; or vice versa. The system can lose more or less
219 heat over the shelf relative to the basin, and thereby form more or less sea ice, without disturbing
220 the balance across section A.

221 Next consider Fig. 5, which shows results from experiment 2. This experiment is the same as
222 experiment 1, except that the total ocean heat loss Q is one third higher (Table 2). The mass fluxes
223 across section A, U_2 and U_3 , are similar, $U_3/U_2 \approx 3.8$. The ice export flux for experiment 2 is
224 also similar, $|U_i|/U_1 \approx 0.036$, to experiment 1. Nevertheless, the solution is qualitatively different
225 because it shows strong shelf circulation, cold OW, and weak entrainment ($\Phi = 0.13$). In this
226 experiment, to satisfy the heat budget across section A, the OW is cold. That is achieved by the AW
227 flowing onto the shelf, where it is cooled to freezing, and then flowing off the shelf to form OW with
228 little entrainment. The system cannot satisfy the heat budget with a weak shelf circulation, warm
229 OW, and strong entrainment, like in experiment 1. By switching to this other mode of solution
230 (strong shelf circulation), the system accommodates the greater ocean heat loss.

231 Now consider Fig. 6, which shows results from experiment 3. This experiment extends experi-
232 ments 1 and 2 to cover a wide range of Q values (Table 2). Fig. 6 shows the key solution variables
233 as functions of Q . In each panel, the thick lines show the solution with entrainment closest to
234 the mean entrainment (like the bars in Figs. 4 and 5). The coloured patches show the range of
235 possible solutions (like the error bars in Figs. 4 and 5). Experiments 1 and 2 are shown with
236 solid and dashed lines, respectively. Notice first that the entrainment Φ (bottom panel of Fig. 6)
237 reflects the shelf circulation switching on (small Φ) and off (large Φ) according to Q . Large Q

238 demands strong shelf circulation to supply a large heat flux from the AW to SW to OW conversion
 239 process. Second, notice that the range of possible solutions is relatively small for experiments 1
 240 and 2, but between them, at $Q/(\rho_i L' U_1) \approx 0.09$, it is large. In this case, the relative strengths of the
 241 shelf circulation and of the PW/OW mass flux ratio are essentially unconstrained (see section 3d).
 242 Finally, notice that the range of possible solutions shrinks to zero for small and large Q (to the left
 243 and right of experiments 1 and 2 in Fig. 6, respectively). At these limits U_2 approaches zero and
 244 for $Q/(\rho_i L' U_1) \lesssim 0.07$ or $Q/(\rho_i L' U_1) \gtrsim 0.11$, no negative U_2 solutions are possible. The system
 245 no longer makes PW—the hatched regions in Fig. 6—and the estuarine circulation collapses.

246 *b. Collapse of the Estuarine Overturning Cell: Heat and Salt Crises*

247 Collapse of the estuarine circulation can occur for two reasons. For small Q , similar to experiment
 248 1, the shelf circulation is switched off, entrainment is high, and the OW is warm. This state allows
 249 maximum export of heat with large OW heat export $-U_3 T_3$ to compensate for the weak ocean heat
 250 loss Q . Export of PW or sea ice effectively carries away negative heat, or equivalently imports
 251 positive heat to the system (because PW is at the freezing temperature and sea ice is deficient in
 252 heat; recall the heat budget is constructed relative to 0°C). Hence, the only way to increase heat
 253 export is to increase $-U_3 T_3$. An upper limit to OW temperature T_3 exists, however, which is set
 254 by aW temperature T_a (supplement sections S4 and S5). Near this limit (large Φ) the system must
 255 compensate for decreased Q by increased OW export $-U_3$. This compensation can only continue
 256 as long as the OW mass flux does not exceed the AW mass flux, $-U_3/U_1 \lesssim 1$, otherwise the PW
 257 flux vanishes. This failure mode (meaning loss of viable solutions) is referred to as *heat crisis*
 258 because the system can no longer export enough heat and also maintain the estuarine circulation.

259 The second reason for collapse of estuarine circulation concerns large Q , similar to experiment
 260 2. In this case, the shelf circulation is switched on, entrainment is low, and OW is near the freezing

261 temperature. This state restricts the export of heat in the thermal cell to supply the large surface
 262 heat loss $Q \approx Q_s$. Restricting the export of heat might instead be accomplished by large U_2 and
 263 small U_3 (because their temperatures are both freezing). But OW is saltier than PW $S_3 > S_2$, so
 264 large U_3 and small U_2 is more efficient at exporting salt. In this state ($U_3 \gg U_2$), greater ocean heat
 265 loss Q can be accommodated by more freezing u_i . More freezing necessarily reduces u_s and hence
 266 U_3 , however, which chokes the export of salt (because sea ice carries very little salt $S_i \ll S_3$). In
 267 trying to meet these competing constraints as Q increases, the system is pushed to vanishing U_2
 268 and collapse of the estuarine circulation. This failure mode is referred to as *salt crisis* because the
 269 system can no longer export enough salt and also maintain the estuarine circulation.

270 *c. Tradeoff between Entrainment and Shelf Circulation*

271 In Figs. 4 and 5 (experiments 1 and 2) we see solutions with similar thermal and estuarine
 272 circulations. In both of them, the OW flux dominates the PW flux by a factor of $U_3/U_2 \approx 3.5$,
 273 which is moderately realistic. The shelf circulation strength u_s differs by a factor of about 14
 274 between the experiments, however. Understanding how experiments 1 and 2 maintain the same
 275 OW/PW ratio despite the large shelf circulation difference illuminates the model.

276 Figure 7 shows entrainment Φ against shelf salinity S_s for experiments 1 and 2 (dots). The
 277 solid curve comes from a theoretical argument about the tradeoff between these two variables (see
 278 supplement section S2). For constant U_3 ,

$$\Phi = 1 - \frac{\gamma^{3/2}}{\rho_0 \beta \Delta S_s} |U_3|^{1/2}, \quad (28)$$

279 which says that the shelf salinity anomaly ΔS_s and (one minus the) entrainment are inversely
 280 proportional to each other. This gives a good fit to the tradeoff between Φ and S_s at fixed U_3 (see
 281 Fig. 7). Physically, it reflects the fact that the AW to OW conversion pathway can either occur by

282 strong entrainment and weak shelf circulation (experiment 1) or vice versa (experiment 2). AW can
283 either flow directly into OW through entrainment or it can circulate on the shelf before becoming
284 OW. As experiments 1 and 2 show, this tradeoff is important for the heat budget, however. Small
285 (large) Q requires export of warm (cold) OW and therefore a weak (strong) shelf circulation.

286 *d. Unconstrained OW/PW Fluxes: OW Emergency*

287 A variation of this idea explains the wide range of possible solutions for intermediate Q , between
288 experiments 1 and 2 in Fig. 6 (see also supplement section S5). For $Q/(\rho_i L' U_1) \approx 0.09$, the ratio
289 of OW/PW fluxes U_3/U_2 is essentially unconstrained. In this case, the system supports solutions
290 with strong OW flux and weak PW flux that have weak entrainment, strong shelf circulation and
291 cold OW. These solutions are far from the solid curves in Fig. 6, although still within the coloured
292 patches (to balance mass, U_2 must be anti-correlated with U_3 at fixed Q , as seen from the solid
293 lines). This shelf-dominated mode efficiently supplies AW heat to the shelf and hence to the
294 atmosphere via Q_s , like experiment 2. But the system also supports solutions with weak OW
295 flux and strong PW flux (unlike experiments 1 and 2). This intermediate- Q mode balances the
296 heat budget by converting AW mainly to PW (which is cold) and suppressing the export of warm
297 OW. It can have either strong or weak entrainment and shelf circulation: the difference between
298 them is unimportant because little AW is converted to OW in the intermediate mode. This type of
299 solution allows vanishing of the OW thermal overturning cell, $U_3 = 0$, as the solid curve shows for
300 $Q/(\rho_i L' U_1) \approx 0.09$. It is called an *OW emergency*: the thermal cell can disappear, but it does not
301 have to disappear (in contrast, recall that the heat and salt crises require collapse of the estuarine
302 cell). See ahead to section 3j and Fig. 11 for an example of an intermediate- Q solution and OW
303 emergency.

304 *e. Sensitivity to Other System Parameters*

305 Experiments 1, 2, and 3 differ only in Q , the ocean heat loss flux. What about sensitivity
 306 to other system parameters? Experiment 4 (Table 2) systematically varies $\{Q, \mathcal{F}, U_1, T_1, S_1\}$ in
 307 1769472 different combinations ($\phi = 0.33$ is held constant: section 3g explores this parameter).
 308 Experiment 4 spans the space of parameters for the Fram Strait and Barents Sea Opening, arising
 309 from uncertainty or secular variability. Fig. 8 shows the results for the export volume fluxes. The
 310 figure shows histograms of the volume fluxes plotted against

$$\mathcal{N}^* \equiv (1 - S_i/S_1)Q + L'\mathcal{F} + \rho_1 c_p (S_i/S_1 - 1)T_1 U_1, \quad (29)$$

$$\approx Q + L\mathcal{F} - \rho_0 c_p U_1 T_1, \quad (30)$$

$$\approx \rho_i L' U_1 (1 + U_2/U_1 + U_3/U_1). \quad (31)$$

311 This compound forcing parameter is a function of (mainly) Q, \mathcal{F} , and $U_1 T_1$. It collapses the
 312 five dimensional $\{Q, \mathcal{F}, U_1, T_1, S_1\}$ parameter space onto a line. Distance along this line, \mathcal{N}^* , is
 313 proportional to Q , but it also depends on the other parameters. In this way, \mathcal{N}^* in experiment 4 and
 314 Fig. 8 generalizes Q in experiment 3 and Fig. 6. The histograms are constructed from the mean
 315 entrainment solutions, like the bars in Fig. 4, and the results from experiment 3 are shown with
 316 white curves on Fig. 8 for reference. Most of the variation in U_2 among the solutions is controlled
 317 by \mathcal{N}^* , indicating that this parameter dominates these variations. Equivalently, for a fixed \mathcal{N}^*
 318 value, the distribution of U_2 values is relatively tight, especially for $U_2 \rightarrow 0$ approaching the heat
 319 and salt crises. For example, the range of U_2 values for fixed \mathcal{N}^* is typically smaller than the range
 320 of U_2 values about the mean entrainment solution seen in Fig. 4. This is a useful result, because
 321 the understanding of the system gained from experiment 3 varying Q alone, carries over to the full
 322 system with varying Q, \mathcal{F}, U_1, T_1 and S_1 . Similar remarks apply to the distribution of U_3 .

323 Physically, $\mathcal{N}^*/(\rho_i L' U_1)$ is the fractional anomaly in the volume budget $U_1 + U_2 + U_3 \approx \mathcal{N}^*/(\rho_i L)$,
 324 meaning that \mathcal{N}^* measures the (small) difference between the AW transport and the OW and PW
 325 transports. Supplement section S3 supports these claims with theoretical arguments, but the main
 326 evidence is that the results of experiment 4 in Fig. 8 plotted against \mathcal{N}^* resemble those from
 327 experiment 3 in Fig. 6 plotted against Q . In particular, the types of solution and failure mode are
 328 the same in experiments 3 and 4.

329 *f. Theory for Parametric Locations of Salt Crisis and OW Emergency*

330 The solution structure in experiments 3 and 4 is determined by the PW crises and the OW
 331 emergency. It is useful to understand and quantify the locations in parameter space that define
 332 these limiting solutions. Specifically, what is the origin of the salt crisis and OW emergency
 333 $Q/(\rho_i L' U_1) \approx 0.11$ and 0.09 values, respectively, seen in Fig. 6 for experiment 3, or of the limiting
 334 values of $\mathcal{N}^*/(\rho_i L' U_1)$ for which $U_2 = 0$, seen in Fig. 8 for experiment 4?

335 Neither the salt crisis nor the OW emergency involve entrainment. For the salt crisis (like
 336 experiment 2), the OW flux is high, the shelf circulation is strong, and entrainment is weak. For
 337 the OW emergency, the OW flux collapses, so entrainment is irrelevant because all the inflowing
 338 AW converts to PW and flows back out. Therefore, the parametric locations of salt crises and OW
 339 emergencies are given by simple functions of the forcing parameters, that can be computed without
 340 solving the model. They avoid non-trivial solution of the entrainment model. Supplement section
 341 S4 shows details, specifically see (S18) and (S19) for the Q values that define the two limiting
 342 solutions. The results of these formulae are plotted in Fig. 9 against the results from experiment 4
 343 for several hundred solutions very close to salt crisis or OW emergency. The theoretical predictions
 344 agree very well with the numerical results.

345 *g. Theory for Parametric Locations of Heat Crisis*

346 What about the heat crises, like the origin of $Q/(\rho_i L' U_1) \approx 0.07$ in Fig. 6, near experiment 1? A
347 non-trivial solution of the entrainment model and the OW properties are now needed. That makes
348 theoretical prediction of the heat crises harder than for salt crises and OW emergencies.

349 Fig. 9 shows three options, depending on different assumptions (supplement section S4 explains
350 the technicalities). The option with least restrictive assumptions is shown with the green patch. It
351 just requires that the system consistently produces OW with a density greater than or equal to the
352 AW density (so that OW flows out of the system beneath AW). The bounds are robust but relatively
353 wide (Fig. 9). The next option requires knowledge of the aW properties (and hence ϕ), but not
354 the shelf salinity. It gives a moderately accurate estimate of the location of the heat crisis for
355 experiment 4, although it is biased low (green circles in Fig. 9). The option with most restrictive
356 assumptions requires knowledge of both the aW properties (ϕ) and the maximum allowed shelf
357 salinity S_s^{\max} (which equals 40 g/kg in all experiments: see section 4). For experiment 4, this
358 option gives an accurate estimate of the parametric location of the heat crisis (green dots in Fig. 9).

359 The mixing fraction ϕ , and especially, the maximum allowed shelf salinity S_s^{\max} , are the weakest
360 parts of the model because they are the most uncertain and ad hoc. The processes that determine ϕ
361 and S_s^{\max} are beyond the scope of this simple model. Therefore, the theoretical constraints possible
362 on the location of heat crises with various assumptions are reported. Nevertheless, even the option
363 with no assumptions about ϕ and S_s^{\max} (green patch in Fig. 9) is useful because it restricts the
364 \mathcal{N}^* parametric location of heat crises. It also quantifies the dependence of the heat crisis on the
365 different forcing parameters (see formula (S20)). This information informs future work on more
366 realistic models that specify ϕ and S_s^{\max} . For further discussion see section 4.

367 *h. Sensitivity to PW salinity S_2 and Mixing Fraction ϕ : Entrainment Emergency*

368 Recall, that the AW to PW conversion model (section 2) sets an upper limit for the PW salinity.
369 In all experiments shown so far, the PW salinity S_2 equals this limit from (22). This assumption is
370 now relaxed, as is the related assumption that aW has a fixed mixing fraction ϕ .

371 Figure 10 shows results for experiment 5, which varies S_2 with all other parameters fixed as for
372 experiment 1 (Table 2). There exists a range of possible solutions at moderate entrainment values.
373 As S_2 decreases, the estuarine cell strength U_2 weakens as for the salt and heat crises. For a certain
374 $S_2 \approx 33.5$ g/kg, U_2 vanishes and the estuarine cell disappears. This crisis differs from the salt
375 and heat crises, however, because entrainment $\Phi \approx 0.63$. It is called an *entrainment emergency*.
376 Approaching the entrainment emergency, the aW salinity S_a decreases because the PW salinity S_2
377 is decreasing. The OW salinity S_3 therefore also decreases. The OW salinity can only decrease
378 until the OW density ρ_3 equals the AW density ρ_1 , however, otherwise the stable stratification of
379 AW above OW fails. Therefore, a crisis occurs beyond which entrainment of aW into overflowing
380 shelf water to form OW is no longer possible. The aW becomes too light (fresh) for solutions to
381 the entrainment model to exist. This entrainment emergency also occurs for large ϕ values that
382 make the aW too fresh, for the same reason (see supplement Fig. S1d).

383 *i. Theory for Parametric Location of Entrainment Emergency*

384 The entrainment emergency is understood by noticing that a maximum OW salinity exists, S_3^{\max}
385 (see supplement section S6):

$$S_3^{\max} \approx S_a + \frac{\gamma^{3/2} |U_1|^{1/2}}{\rho_0 \beta}. \quad (32)$$

386 This value minimizes entrainment Φ with a strong thermal overturning cell, $U_3 \approx -U_1$, and a small
 387 aW/OW density difference. Similarly, a minimum OW temperature exists, T_3^{\min} :

$$T_3^{\min} = T_a - (T_a - T_f) \frac{\gamma^{3/2} |U_1|^{1/2}}{\rho_1 - \rho_a}. \quad (33)$$

388 In practice, S_3^{\max} is a more stringent restriction than T_3^{\min} (see the green patches in Figs. 4 and
 389 5). As the aW gets fresher and/or warmer (therefore less dense), these restrictions get tighter.
 390 Eventually, the maximum OW salinity equals the minimum allowed OW salinity to keep OW
 391 denser than AW. At that point the entrainment emergency is reached.

392 The aW properties controlling these restrictions depend on ϕ and S_2 . In experiment 5, S_2 is
 393 decreased until the entrainment emergency occurs for $S_2 \approx 33.5$ g/kg. The corresponding aW
 394 temperature and salinity are $T_a = 1.68^\circ\text{C}$ and $S_a = 34.5$ g/kg. From (32), $S_3^{\max} \approx 34.78$ g/kg,
 395 very close to the value from the numerical solution of $S_3 = 34.70$ g/kg, as seen in Fig. 10. The
 396 corresponding OW temperature is $T_3 = 0.35^\circ\text{C}$ (so that $\rho_3 = \rho_1$) and the entrainment fraction is
 397 $\Phi = (T_3 - T_f)/(T_a - T_f) \approx 0.63$ from (18), as seen in Fig. 10.

398 *j. Antarctic Reference Solution and Choice of γ*

399 Figure 11 shows a canonical Antarctic solution (experiment 6). The parameters (Table 2) are
 400 $U_1 = 26$ Sv (Abernathey et al. 2016), $T_1 = 0.5^\circ\text{C}$, $S_1 = 34.84$ g/kg (Price and O’Neil Baringer
 401 1994), $Q = 300$ TW (Volkov et al. 2010), and $\mathcal{F} = -240 \times 10^6$ kgs⁻¹ (Abernathey et al. 2016). As
 402 for the Arctic solutions, these are representative values with substantial variability and uncertainty.
 403 They represent (crudely) the meridional overturning circulation at all longitudes, consistent with
 404 the paradigm of zonal-average overturning in the Southern Ocean (Talley 2013; Abernathey et al.
 405 2016; Pellichero et al. 2018). The solution in Fig. 11 has a wide range of OW water properties,
 406 entrainment values, and shelf salinities. The canonical solution has $U_2 \approx -16$ Sv, $U_3 \approx -10$ Sv,

407 and $u_i \approx -0.27$ Sv, which are moderately realistic values (Abernathey et al. 2016; Pellichero et al.
 408 2018). The PW flux nearly always exceeds the OW flux and the system is close to OW emergency.
 409 In this sense, the system is more loosely constrained than experiments 1 and 2 and further from
 410 heat and salt crises. It is close to switching between strong and weak shelf circulation (Fig. 6).

411 The Antarctic reference solution reveals an important issue, namely, the choice of entrainment
 412 parameter γ from (17). Recall from section 2a that γ sets the sensitivity of entrainment to changes
 413 in overflowing SW flux and density difference:

$$\gamma = \frac{\rho_0^{2/3} f}{g^{2/3} \alpha_{\max} (W_s + 2K_{\text{geo}}x)^{1/3}}. \quad (34)$$

414 For the Arctic experiments 1–5, $\gamma = 2.2 \times 10^{-3} \text{ kg}^{2/3} \text{ s}^{1/3} \text{ m}^{-3}$, which derives from Price and O’Neil
 415 Baringer (1994) (their Table 1). The main γ uncertainty is in $W_s + 2K_{\text{geo}}x$, where W_s is the overflow
 416 plume width, K_{geo} is the geostrophic Ekman number, and x is downstream distance. This sum
 417 is dominated by the plume width W_s for the cases shown here, so focus on W_s . How should
 418 W_s vary with the inflow flux U_1 , which sets the circulation scale for the problem? The simplest
 419 choice, adopted here, is to make W_s proportional to U_1 . Physically, that means the shelf system
 420 can accommodate arbitrarily broad overflow plumes (technically, it means the problem is linear
 421 in U_1). This choice cannot be true for all possible U_1 fluxes of course because of the limits on
 422 the length of the shelf break (and the $2K_{\text{geo}}x$ term). But for experiments 1 and 6, $W_s = 100$ and
 423 550km, respectively, which are short compared to the lengths of the Siberian and Antarctic shelves
 424 so the choice appears plausible. In any case, γ has little effect on salt crises because entrainment
 425 vanishes for them, or on the possibility of OW emergencies.

4. Discussion

Fig. 12 shows a schematic of the main solution modes for this model, summarizing section 3. The quantitative details of the experiments depend on specific parameter choices, but the qualitative solution modes do not. These modes are organized by PW collapse (loss of the estuarine cell) in heat and salt crises; by unconstrained tradeoff between PW and OW in OW emergency (possible loss of the overturning cell); and by entrainment emergency (loss of the estuarine cell). The transition between these modes is mainly controlled by the compound forcing parameter \mathcal{N}^* (section 3e, eqs. (29)–(31)), which generalizes the effect of the ocean heat loss rate Q . The \mathcal{N}^* parameter estimates the departure from the closed volume budget between AW, OW, and PW. For example, heat crises relate to relatively small OW plus PW transport, indicating relatively large sea ice export. But that occurs for small \mathcal{N}^* (Figs. 4, 6, 9), which is associated with little freezing because the ocean heat loss rate Q is small. Therefore, a contradiction arises, which is the heat crisis. Similarly, salt crises relate to relatively large OW plus PW transport, indicating small sea ice export, but they occur for large Q . For intermediate \mathcal{N}^* values (near zero), the ratio of OW to PW is loosely constrained because the system can switch between strong and weak shelf circulation strengths (with concomitant weak and strong entrainment). Indeed, the thermal cell can disappear in an OW emergency because the constraints are so loose.

The entrainment emergency is different because it does not mainly depend on \mathcal{N}^* . Entrainment emergencies relate to entrained aW becoming too fresh (not dense enough), such as when PW is too fresh. Our approach is to prescribe the aW and PW properties without specifying the physical formation process. The assumption is that the system can freely select aW properties. Therefore, the system can avoid entrainment emergencies by suitable aW and PW choices. In other words, the entrainment emergency does not constrain the possible solution modes for this model, but it

449 does constrain possible aW and PW properties. These constraints are potentially useful because
450 they can be tight, for example on the minimum allowed PW salinity (Fig. 10).

451 The sign of the solution sensitivity to forcing parameters depends on the solution location
452 with respect to the crises and emergencies. For example, the estuarine PW cell strengthens as Q
453 increases if entrainment dominates and OW is warm (like experiment 1 in Fig. 6). But the estuarine
454 cell weakens as Q increases if shelf circulation dominates and OW is cold (like experiment 2).
455 The sensitivity of the sea ice export flux to Q also changes sign like this (Figs. 6 and 8). OW
456 thermohaline properties are insensitive to forcing parameters, except when the system switches
457 between strong and weak shelf circulation near the OW emergency. Then, the OW temperature
458 (but not salinity) is very sensitive to forcing changes, which leads to a bimodal distribution of OW
459 temperature (Fig. 6). The OW properties are buffered to changes in shelf salinity in this way. The
460 corollary is that the shelf salinity is relatively unconstrained by the OW properties reflecting the
461 tradeoff between entrainment and shelf circulation (Fig. 7).

462 The \mathcal{N}^* forcing parameter shows that solution sensitivity depends (essentially) on the individual
463 forcing parameters in a straightforward way (eq. (29)). Specifically, Q changes and freshwater
464 flux changes are interchangeable: greater ocean heat loss compensates greater ocean freshwater
465 gain, and vice versa. Similarly, only the difference between Q and AW heat flux matters, not the
466 individual magnitudes, and the AW salt flux is unimportant. These results emerge from the mass,
467 salt, and heat budgets so they are robust.

468 The main approximation in this model is the Price and O’Neil Baringer (1994) entrainment
469 parametrization. In particular, uncertainty surrounds the functional form (17), the entrainment
470 sensitivity parameter γ , the maximum shelf salinity S_s^{\max} , and the aW properties (from PW salinity
471 S_2 and mixing fraction ϕ). Still, the entrainment model is based on firm physical principles. Price
472 and O’Neil Baringer (1994) couple entrainment to the dynamics of the overflow plume, which is

473 the key ingredient in the present model. Their parametrization says that the dense SW overflowing
474 the shelf break is geostrophic, spreads due to Ekman drainage at the sea floor, and mixes with
475 aW in hydraulic jumps. It makes sense that increasing entrainment depends on increasing SW/aW
476 density difference in (17) because the geostrophic current is proportional to the density difference.
477 It is less obvious that increasing entrainment depends on decreasing SW transport (albeit weakly).
478 The reason is that a larger transport means a thicker overflow plume and therefore a smaller Froude
479 number (because the wave speed increases with plume thickness) and less entrainment. Price and
480 O’Neil Baringer (1994) are guided by the laboratory experiments of Ellison and Turner (1959) and
481 Turner (1986). These studies suggest that mixing during entrainment events is so efficient that the
482 Froude number cannot exceed one. The assumption of geostrophic flow, and thus a geostrophic
483 Froude number in (8), implies the two-thirds exponent in the Froude number scaling (7) (J. Price,
484 pers. comm.). A different exponent would change the details of the switch between strong and weak
485 shelf circulation magnitudes, but not the existence of the switching. Other studies on overflow
486 entrainment point to the importance of entrainment for subcritical flows (Froude number <1 ,
487 Cenedese and Adduce 2010), especially over rough bottoms (Ottolenghi et al. 2017). Boosting of
488 entrainment by tidal currents is also thought to be important in some situations, such as for AABW
489 in the Ross Sea (Padman et al. 2009). These additional effects are worth exploring, but appear
490 unlikely to make a qualitative difference. The reason is that few solutions have subcritical flow and
491 vanishing entrainment (Figs. 6, 8). On these grounds, the main solution modes in Figs. 6 and 12
492 probably just require that entrainment grows sensitively with Froude number.

493 Consider now the maximum SW salinity S_s^{\max} (see section 3g and supplement section S1). This
494 parameter is unavoidable in the numerical method because the entrainment parametrization (17)
495 involves a power law of the aW/SW density (hence salinity) difference. Therefore, no characteristic
496 maximum shelf salinity exists. The upper limit on SW salinity is controlled in reality by other

497 processes. Most important is exchange across the shelf break jet unrelated to dense overflows,
498 like baroclinic instability (Lambert et al. 2018; Stewart et al. 2018). This exchange augments
499 dense overflows in exporting salt from the shelf (and importing heat on to the shelf). The relative
500 importance of these shelf break exchange mechanisms and their interaction are unclear and worth
501 exploring. The key question is how they control (in order of priority) the OW temperature, OW
502 salinity, and PW salinity because once these variables are known, the budget equations (S1) specify
503 the transports. Despite the uncertainty in what sets S_s^{\max} , the results from experiment 5 with a wide
504 range of forcing parameters show that the value chosen here is unimportant: The mean, median,
505 and modal excess SW salinities over AW salinities are just 0.67, 0.04, and -0.06 g/kg, respectively.
506 These are reasonable values compared to the observations mentioned in section 1.

507 Several other potentially important processes are excluded. Among them are pressure-dependent
508 effects in seawater density, such as thermobaricity (Killworth 1977; Stewart and Haine 2016). The
509 seawater thermodynamic calculations are at zero pressure in these experiments. This approximation
510 is most suspect for the aW/SW entrainment parametrization as that process occurs at depth on the
511 continental slope. Correcting for thermobaricity would increase the SW density relative to the
512 aW density (because SW is colder and cold water is more compressible). That effect enhances
513 entrainment for the reasons given above, although it is probably small as the entrainment does
514 not occur at great depths. Cabbeling is also ignored, which is important for mixing at strong
515 thermohaline fronts (Stewart et al. 2017) and potentially for upwelling of CDW in the Southern
516 Ocean (Evans et al. 2018). Cabbeling creates anomalously dense water by mixing due to the
517 curvature of isopycnals in thermohaline coordinates (see Fig. 3). The linear mixing formulae (like
518 (13)–(15)) include it, but the impact on stratifying the water column is beyond the scope of this
519 layer model. Interaction with ice sheets is also potentially important, especially in the Antarctic
520 where glacial melt is significant (Jenkins et al. 2016; Abernathy et al. 2016; Dinniman et al.

2016). This source of freshwater depends on the ocean heat flux to the ice sheet, but the freshwater flux is specified here, regardless of the shelf circulation. Indeed, both the freshwater flux and the ocean heat loss flux Q are specified independently of the system state. They are also allowed to freely vary between shelf and basin, with only their sums constrained (supplement section S1). These assumptions are unrealistic because Q , for instance, depends on sea ice cover. Refining these assumptions is beyond the present scope, partly because it requires more geometric parameters, like shelf area and depth: in the present model, the sea ice flux and sea ice thickness and concentration, which control Q , are not linked.

Only steady solutions are shown, but in the real system time-dependent solutions may be important too, and they are intrinsically interesting. For time-dependence the model equations must be expanded to include water mass reservoir volumes, which will control the characteristic time scales for transient adjustment. One possibility is to couple the shelf and basin so they can exchange heat and salt anomalies. This coupling may resolve the degeneracy near the OW emergency into periodic solutions. Conceptually, it is easy to build an oscillator by adding negative feedback. Think of the OW temperature T_3 as a function of $N^* \approx Q + L\mathcal{F} - c_p\rho_1T_1U_1$ (from (29)). The OW temperature is high for low Q (or N^*) from Fig. 6 (or 8), and vice versa, so the system output T_3 inverts the input signal N^* . Allowing the OW temperature to control N^* , by making U_1 depend on $T_1 - T_3$, for example, will trigger self-sustained oscillations. This mechanism has been proposed for low-frequency Atlantic Meridional Overturning Circulation variability because U_1 depends on $T_1 - T_3$ via the thermal wind relation (see Haine 2016 for a commentary and references therein).

5. Conclusions

This paper reports a conceptual model that specifies the strengths and thermohaline properties of polar estuarine and thermal overturning cells. The model satisfies mass, salt, and heat budgets

544 plus physical parametrizations for PW and OW formation. We explore the model characteristics
545 and apply it to the Arctic and Antarctic termini of the global ocean overturning circulation. At
546 best, the conceptual model is a caricature of a piece of the real system. It is most useful where
547 it suggests characteristics of the estuarine and thermal overturning cells that are robust in more
548 realistic models. Then it guides further research. The salient model characteristics are:

- 549 • The system is controlled by five flux parameters, namely the inflowing mass, heat, and fresh-
550 water fluxes, and the air/sea/ice heat and freshwater fluxes. However, the state is dominated
551 by a single forcing parameter (eq. (29)) that is a linear combination of ocean heat loss flux,
552 inflowing heat flux and ocean freshwater flux. This parameter measures the departure from a
553 balanced volume budget between the estuarine and thermal overturning cells.
- 554 • A one-parameter infinity of solutions typically exists but the range of possible solutions can
555 be tight. The solutions have different circulations onto and off the continental shelf, which
556 links to overflow entrainment. This tradeoff permits switching between two states: the states
557 exhibit strong (weak) shelf circulation, weak (strong) overflow entrainment, and large (small)
558 heat flux from the ocean to the atmosphere. Switching allows the system to accommodate a
559 wide range of inflow and air/sea/ice exchange fluxes and gives a bi-modal distribution of OW
560 temperature with a narrow range of OW salinity.
- 561 • Solutions exist for limited flux parameters. Solutions disappear if the heat (salt) budget fails to
562 balance because the system cannot export enough heat (salt). These heat (salt) crises collapse
563 the estuarine cell. The thermal overturning cell is robust meaning that it can collapse in a
564 so-called OW emergency, but it does not have to.
- 565 • For the Arctic, specifically the transfer across the Fram Strait and Barents Sea Opening,
566 the real system appears vulnerable to heat crisis. The estuarine cell vanishes for increased

567 meteoric freshwater flux to the ocean, or increased AW heat flux, or decreased ocean heat loss
568 flux. The first two factors are anticipated under global warming (Rawlins et al. 2010; Vavrus
569 et al. 2012; Collins et al. 2013), pushing the Arctic closer to heat crisis and collapse of the
570 estuarine cell. This may relate to Arctic Ocean “Atlantification” (Polyakov et al. 2017).

- 571 • For the Antarctic, the real system appears close to OW emergency with weak constraints on the
572 strengths of the estuarine and thermal cells, although most solutions show a stronger estuarine
573 cell. This result suggests that the Antarctic system is more susceptible to unforced variations
574 than the Arctic. The sensitivity of the Antarctic solutions to changes in flux parameters
575 is unclear because the system appears close to switching between strong and weak shelf
576 circulation modes. Loss of parts of the estuarine cell may relate to loss of sea ice and PW
577 in Weddell Sea polynyas (Comiso and Gordon 1987; Gordon 2014). Such offshore polynyas
578 are linked to climate variations that are projected to strengthen with anthropogenic climate
579 change (Campbell et al. 2019). Loss of the thermal cell may relate to loss of AABW formation
580 in future climate projections (Lago and England 2019).

581 The most important lessons from this conceptual polar overturning model are probably these:
582 The Arctic system is being driven towards heat crisis and collapse of the estuarine overturning
583 cell by flux changes associated with anthropogenic climate change. Approaching the heat crisis,
584 entrainment and shelf salinity are high, shelf circulation is weak, and variability in OW flux and
585 temperature is small. Sea ice does not disappear prior to the heat crisis. The Antarctic system
586 occupies a regime with large intrinsic variability between OW and PW fluxes and between strong
587 and weak shelf circulations. The magnitude and sign of the sensitivity to changes in ocean heat
588 loss, freshwater gain, and CDW heat flux are uncertain.

589 *Data availability statement.* The MATLAB software to compute solutions to the
590 conceptual model in this paper is available at [https://github.com/hainegroup/
591 Polar-overturning-circulation-model](https://github.com/hainegroup/Polar-overturning-circulation-model). An interactive app and the scripts to produce the
592 figures are available.

593 *Acknowledgments.* This work was supported by grant 19-PO19-0025 from the National Aeronau-
594 tics and Space Administration. Discussions with Ali Siddiqui, Miguel Jimenez-Urias, and Renske
595 Gelderloos helped clarify the work and Bert Rudels inspired it.

596 **References**

597 Aagaard, K., L. K. Coachman, and E. Carmack, 1981: On the halocline of the Arctic Ocean. *Deep
598 Sea Res., Part A*, **28 (6)**, 529–545, doi:10.1016/0198-0149(81)90115-1.

599 Aagaard, K., J. H. Swift, and E. C. Carmack, 1985: Thermohaline circulation in the Arctic
600 Mediterranean Seas. *J. Geophys. Res.*, **90 (C3)**, 4833, doi:10.1029/jc090ic03p04833.

601 Abernathey, R. P., I. Cerovecki, P. R. Holland, E. Newsom, M. Mazloff, and L. D. Talley, 2016:
602 Water-mass transformation by sea ice in the upper branch of the Southern Ocean overturning.
603 *Nature Geoscience*, **9 (8)**, 596–601, doi:10.1038/ngeo2749.

604 Boyer, T. P., and Coauthors, 2018: World ocean database 2018. Tech. rep., NOAA Atlas NESDIS
605 87. https://data.nodc.noaa.gov/woa/WOD/DOC/wod_intro.pdf.

606 Campbell, E. C., E. A. Wilson, G. W. K. Moore, S. C. Riser, C. E. Brayton, M. R. Mazloff, and L. D.
607 Talley, 2019: Antarctic offshore polynyas linked to Southern Hemisphere climate anomalies.
608 *Nature*, **570 (7761)**, 319–325, doi:10.1038/s41586-019-1294-0.

609 Cenedese, C., and C. Adduce, 2010: A new parameterization for entrainment in overflows.
610 *J. Phys. Oceanogr.*, **40 (8)**, 1835–1850, doi:10.1175/2010jpo4374.1.

- 611 Collins, M., and Coauthors, 2013: Long-term climate change: Projections, commitments and
612 irreversibility. *Climate Change 2013: The Physical Science Basis. Contribution of Working*
613 *Group I to the Fifth Assessment Report of the Intergovernmental Panel on Climate Change*, T. F.
614 Stocker, D. Qin, G.-K. Plattner, M. Tignor, S. K. Allen, J. Boschung, A. Nauels, Y. Xia, V. Bex,
615 and P. M. Midgley, Eds., Cambridge University Press, Cambridge, United Kingdom and New
616 York, NY, USA.
- 617 Comiso, J. C., and A. L. Gordon, 1987: Recurring polynyas over the Cosmonaut Sea and the Maud
618 Rise. *J. Geophys. Res.*, **92 (C3)**, 2819, doi:10.1029/jc092ic03p02819.
- 619 Dinniman, M., X. Asay-Davis, B. Galton-Fenzi, P. Holland, A. Jenkins, and R. Timmermann,
620 2016: Modeling ice shelf/ocean interaction in Antarctica: A review. *Oceanography*, **29 (4)**,
621 144–153, doi:10.5670/oceanog.2016.106.
- 622 Eldevik, T., and J. E. Ø. Nilsen, 2013: The Arctic–Atlantic thermohaline circulation. *J. Climate*,
623 **26 (21)**, 8698–8705, doi:10.1175/jcli-d-13-00305.1.
- 624 Ellison, T. H., and J. S. Turner, 1959: Turbulent entrainment in stratified flows. *J. Fluid Mech.*,
625 **6 (03)**, 423, doi:10.1017/s0022112059000738.
- 626 Evans, D. G., J. D. Zika, A. C. Naveira Garabato, and A. J. G. Nurser, 2018: The cold
627 transit of Southern Ocean upwelling. *Geophys. Res. Lett.*, **45 (24)**, 13,386–13,395, doi:
628 10.1029/2018gl079986.
- 629 Foster, T. D., and E. C. Carmack, 1976: Frontal zone mixing and Antarctic bottom water formation
630 in the southern Weddell Sea. *Deep Sea Res.*, **23**, 301–317.
- 631 Gill, A. E., 1973: Circulation and bottom water production in the Weddell Sea. *Deep Sea Res.*, **20**,
632 111–140, doi:10.1016/0011-7471(73)90048-x.

- 633 Gordon, A. L., 2014: Southern Ocean polynya. *Nature Climate Change*, **4** (4), 249–250, doi:
634 10.1038/nclimate2179.
- 635 Haine, T. W. N., 2016: Ocean science: Vagaries of Atlantic overturning. *Nature Geoscience*, **9**,
636 479–480, doi:10.1038/ngeo2748.
- 637 Haine, T. W. N., and Coauthors, 2015: Arctic freshwater export: Status, mechanisms, and
638 prospects. *Glob. Planet. Change*, **125**, 13–35, doi:10.1016/j.gloplacha.2014.11.013.
- 639 Hansen, B., and S. Østerhus, 2000: North Atlantic-Nordic Seas exchange. *Prog. Oceanogr.*, **45**,
640 109–208.
- 641 Hansen, B., S. Østerhus, W. R. Turrell, S. Jónsson, H. Valdimarsson, H. Hátún, and S. M. Olsen,
642 2008: The inflow of Atlantic water, heat, and salt to the Nordic Seas across the Greenland-
643 Scotland ridge. *Arctic-Subarctic Ocean Fluxes: Defining the role of the Northern Seas in*
644 *Climate*, R. R. Dickson, J. Meincke, and P. Rhines, Eds., Springer-Verlag, 15–43, doi:10.1007/
645 978-1-4020-6774-7_2.
- 646 Jacobs, S. S., 2004: Bottom water production and its links with the thermohaline circulation.
647 *Antarctic Science*, **16** (4), 427–437, doi:10.1017/s095410200400224x.
- 648 Jenkins, A., P. Dutrieux, S. Jacobs, E. Steig, H. Gudmundsson, J. Smith, and K. Heywood, 2016:
649 Decadal ocean forcing and Antarctic ice sheet response: Lessons from the Amundsen Sea.
650 *Oceanography*, **29** (4), 106–117, doi:10.5670/oceanog.2016.103.
- 651 Killworth, P. D., 1977: Mixing on the Weddell Sea continental slope. *Deep Sea Res.*, **24**, 427–448.
- 652 Klinger, B. A., and T. W. N. Haine, 2019: *Ocean Circulation in Three Dimensions*. 1st ed.,
653 Cambridge University Press, Cambridge, United Kingdom and New York, NY, USA, URL
654 <http://www.cambridge.org/9780521768436>.

655 Lago, V., and M. H. England, 2019: Projected slowdown of Antarctic bottom water formation
656 in response to amplified meltwater contributions. *J. Climate*, **32** (19), 6319–6335, doi:10.1175/
657 jcli-d-18-0622.1.

658 Lambert, E., T. Eldevik, and M. A. Spall, 2018: On the dynamics and water mass transformation of
659 a boundary current connecting alpha and beta oceans. *J. Phys. Oceanogr.*, **48** (10), 2457–2475,
660 doi:10.1175/jpo-d-17-0186.1.

661 Marshall, J., and K. Speer, 2012: Closure of the meridional overturning circulation through
662 Southern Ocean upwelling. *Nature Geoscience*, **5**, 171–180, doi:10.1038/ngeo1391.

663 Maus, S., 2003: Interannual variability of dense shelf water salinities in the north-western Barents
664 Sea. *Polar Research*, **22** (1), 59–66, doi:10.3402/polar.v22i1.6444.

665 Muench, R., L. Padman, A. Gordon, and A. Orsi, 2009: A dense water outflow from the Ross
666 Sea, Antarctica: Mixing and the contribution of tides. *J. Mar. Res.*, **77** (4), 369–387, doi:
667 10.1016/j.jmarsys.2008.11.003.

668 Naveira Garabato, A. C., E. L. McDonagh, D. P. Stevens, K. J. Heywood, and R. J. Sanders, 2002:
669 On the export of Antarctic Bottom Water from the Weddell Sea. *Deep Sea Res., Part II*, **49** (21),
670 4715–4742, doi:10.1016/s0967-0645(02)00156-x.

671 Orsi, A. H., G. C. Johnson, and J. L. Bullister, 1999: Circulation, mixing, and production of
672 Antarctic bottom water. *Prog. Oceanogr.*, **43**, 55–109, doi:10.1016/s0079-6611(99)00004-x.

673 Østerhus, S., W. R. Turrell, S. Jónsson, and B. Hansen, 2005: Measured volume, heat, and salt
674 fluxes from the Atlantic to the Arctic Mediterranean. *Geophys. Res. Lett.*, **32**, doi:10.1029/
675 2004GL022188.

- 676 Ottolenghi, L., C. Cenedese, and C. Adduce, 2017: Entrainment in a dense current flowing
677 down a rough sloping bottom in a rotating fluid. *J. Phys. Oceanogr.*, **47** (3), 485–498, doi:
678 10.1175/jpo-d-16-0175.1.
- 679 Padman, L., S. L. Howard, A. H. Orsi, and R. D. Muench, 2009: Tides of the northwestern Ross
680 Sea and their impact on dense outflows of Antarctic Bottom Water. *Deep Sea Res., Part II*,
681 **56** (13-14), 818–834, doi:10.1016/j.dsr2.2008.10.026.
- 682 Pellichero, V., J.-B. Sallée, C. C. Chapman, and S. M. Downes, 2018: The southern ocean merid-
683 ional overturning in the sea-ice sector is driven by freshwater fluxes. *Nature Communications*,
684 **9** (1), doi:10.1038/s41467-018-04101-2.
- 685 Polyakov, I. V., and Coauthors, 2017: Greater role for Atlantic inflows on sea-ice loss in the Eurasian
686 Basin of the Arctic Ocean. *Science*, **356** (6335), 285–291, doi:10.1126/science.aai8204.
- 687 Price, J. F., and M. O’Neil Baringer, 1994: Outflows and deep water production by marginal seas.
688 *Prog. Oceanogr.*, **33**, 161–200, doi:10.1016/0079-6611(94)90027-2.
- 689 Quadfasel, D., B. Rudels, and K. Kurz, 1988: Outflow of dense water from a Svalbard fjord into
690 the Fram Strait. *Deep Sea Res., Part A*, **35** (7), 1143–1150, doi:10.1016/0198-0149(88)90006-4.
- 691 Rawlins, M. A., and Coauthors, 2010: Analysis of the Arctic system for freshwater cycle intensifica-
692 tion: Observations and expectations. *J. Climate*, **21**, 5715–5737, doi:10.1175/2010JCLI3421.1.
- 693 Rudels, B., 2010: Constraints on exchanges in the Arctic Mediterranean—do they exist and can
694 they be of use? *Tellus*, **62A**, 109–122, doi:10.1111/j.1600-0870.2009.00425.x.
- 695 Rudels, B., 2012: Arctic Ocean circulation and variability - advection and external forcing en-
696 counter constraints and local processes. *Ocean Sci.*, **8**, 261–286, doi:10.5194/os-8-261-2012.

- 697 Rudels, B., 2016: Arctic Ocean stability: The effects of local cooling, oceanic heat transport,
698 freshwater input, and sea ice melt with special emphasis on the Nansen basin. *J. Geophys. Res.*,
699 **121**, doi:10.1002/2015JC011045.
- 700 Rudels, B., E. Fahrbach, J. Meincke, G. Budéus, and P. Eriksson, 2002: The East Greenland
701 Current and its contribution to the Denmark Strait overflow. *ICES J. Mar. Sci.*, **59**, 1133–1154,
702 doi:10.1006/jmsc.2002.1284.
- 703 Rudels, B., and D. Quadfasel, 1991: Convection and deep water formation in the Arctic Ocean-
704 Greenland Sea system. *J. Mar. Sys.*, **2 (3-4)**, 435–450, doi:10.1016/0924-7963(91)90045-v.
- 705 Stewart, A. L., A. Klocker, and D. Menemenlis, 2018: Circum-Antarctic shoreward heat transport
706 derived from an eddy- and tide-resolving simulation. *Geophys. Res. Lett.*, **45 (2)**, 834–845,
707 doi:10.1002/2017gl075677.
- 708 Stewart, K. D., and T. W. N. Haine, 2016: Thermobaricity in the transition zones between alpha
709 and beta oceans. *J. Phys. Oceanogr.*, **46 (6)**, 1805–1821, doi:10.1175/jpo-d-16-0017.1.
- 710 Stewart, K. D., T. W. N. Haine, A. M. Hogg, and F. Roquet, 2017: On cabbelling and thermobaricity
711 in the surface mixed layer. *J. Phys. Oceanogr.*, **47**, 1775–1787, doi:10.1175/jpo-d-17-0025.1.
- 712 Talley, L., 2013: Closure of the global overturning circulation through the Indian, Pacific,
713 and Southern Oceans: Schematics and transports. *Oceanography*, **26 (1)**, 80–97, doi:
714 10.5670/oceanog.2013.07.
- 715 Tamura, T., and K. I. Ohshima, 2011: Mapping of sea ice production in the Arctic coastal polynyas.
716 *J. Geophys. Res.*, **116 (C7)**, doi:10.1029/2010jc006586.

- 717 Tsubouchi, T., and Coauthors, 2012: The Arctic Ocean in summer: A quasi-synoptic inverse
718 estimate of boundary fluxes and water mass transformation. *J. Geophys. Res.*, **117**, C01024,
719 doi:10.1029/2011JC007174.
- 720 Tsubouchi, T., and Coauthors, 2018: The Arctic Ocean seasonal cycles of heat and freshwater
721 fluxes: observation-based inverse estimates. *J. Phys. Oceanogr.*, doi:10.1175/jpo-d-17-0239.1.
- 722 Turner, J. S., 1986: Turbulent entrainment: the development of the entrainment assump-
723 tion, and its application to geophysical flows. *J. Fluid Mech.*, **173**, 431–471, doi:10.1017/
724 s0022112086001222.
- 725 Vavrus, S. J., M. M. Holland, A. Jahn, D. Bailey, and B. A. Blazey, 2012: Twenty-first-century
726 Arctic climate change in CCSM4. *J. Climate*, **25**, 2696–2710, doi:10.1175/JCLI-D-11-00220.1.
- 727 Volkov, D. L., L.-L. Fu, and T. Lee, 2010: Mechanisms of the meridional heat transport in the
728 Southern Ocean. *Ocean. Dyn.*, **60** (4), 791–801, doi:10.1007/s10236-010-0288-0.

729

LIST OF TABLES

730

731

732

Table 1. Table of notation. AW = Atlantic Water (subscript 1), PW = Polar Water (subscript 2), OW = Overflow Water (subscript 3), aW = ambient Water. See also Fig. 2. 39

733

734

Table 2. Table of Experiments. The mixing fraction $\phi = 0.33$; see section 3h for a discussion. For all experiments $\delta\Phi = 0.01$ (see supplement section S1). 40

735 TABLE 1. Table of notation. AW = Atlantic Water (subscript 1), PW = Polar Water (subscript 2), OW =
736 Overflow Water (subscript 3), aW = ambient Water. See also Fig. 2.

Symbol	Unit	Meaning
Parameters		
U_1, T_1, S_1	Sv, °C, g/kg	AW volume flux, temperature, salinity at gateway
$Q = Q_b + Q_s$	W	Ocean heat flux (total = basin + shelf)
$\mathcal{F} = \mathcal{F}_b + \mathcal{F}_s$	kg s ⁻¹	Ocean freshwater flux (total = basin + shelf)
ϕ	(no unit)	Fraction of PW to AW entrained into OW
\mathcal{N}^*	W	Compound forcing parameter from (29)
Variables		
U_2, U_3, U_i	Sv	PW, OW, sea ice volume flux at gateway
u_1, u_i	Sv	AW, sea ice volume flux at shelf break
S_s	g/kg	SW salinity
Intermediate variables		
S_2	g/kg	PW salinity
T_3, S_3	°C, g/kg	OW temperature, salinity
T_a, S_a	°C, g/kg	aW temperature, salinity
u_s	Sv	SW volume flux at shelf break
$\rho_1, \rho_2, \rho_3, \rho_a$	kg m ⁻³	AW, PW, OW, aW density
Φ	(no unit)	Entrainment fraction
Constants		
T_i, S_i	°C, g/kg	Sea ice temperature, salinity
$T_2 = T_s = T_f$	°C	PW, SW, freezing temperature
ρ_i, ρ_0	kg m ⁻³	Sea ice, characteristic seawater density
c_p, c_i	J kg ⁻¹ K ⁻¹	Seawater, sea ice specific heat capacity
L	J kg ⁻¹	Latent heat of fusion
α, β	°C ⁻¹ , kg/g	Thermal expansion, haline contraction coefficients
γ	kg ^{2/3} s ^{1/3} m ⁻³	Entrainment parameter in (17)

737 TABLE 2. Table of Experiments. The mixing fraction $\phi = 0.33$; see section 3h for a discussion. For all
 738 experiments $\delta\Phi = 0.01$ (see supplement section S1).

Experiment	Description	U_1 Sv	T_1 °C	S_1 g/kg	Q TW	$-\mathcal{F}$ $\times 10^9 \text{kg s}^{-1}$
1	Fram Strait+BSO	4.75	3.40	35.00	115	180
2	Fram Strait+BSO high Q	4.75	3.40	35.00	153	180
3	Fram Strait+BSO various Q	4.75	3.40	35.00	87–195	180
4	Fram Strait+BSO various parameters	3.17–7.13	2.55–4.53	34.30–35.70	70–280	75–300
5	Fram Strait+BSO various S_2	4.75	3.40	35.00	115	180
6	Antarctic	26.0	0.50	34.67	300	240

739 **LIST OF FIGURES**

740 **Fig. 1.** Upper two panels: Observations of temperature, salinity and normal geostrophic current
741 across the Fram Strait and Barents Sea Opening. Modified from Klinger and Haine (2019)
742 and based on results from Tsubouchi et al. (2012). Lower panel: Temperature and salinity
743 data from Fram Strait in August 2002 (light gray) and from the Barents Sea Opening in
744 August 2017 (dark gray; from the World Ocean Database, Boyer et al. 2018). 43

745 **Fig. 2.** Schematic of the conceptual polar overturning model. The sign convention is that positive
746 volume fluxes are towards the right. For plausible solutions $\{U_2, U_3, U_i, u_s, u_i\} < 0$ and $u_1 > 0$,
747 as the arrows show. The bathymetric bump at section A (nominally, the Fram Strait and
748 Barents Sea Opening) is for illustrative purposes: the dashed line represents the Antarctic
749 case. Table 1 defines the symbols. 44

750 **Fig. 3.** Schematic of the processes affecting OW properties. The Atlantic Water (AW) properties are
751 specified. The Polar Water (PW) properties are freezing temperature and salinity less than
752 the maximum value given by the dotted line tangent to the AW isopycnal. The ambient Water
753 (aW) properties are a mixture of PW and AW determined by ϕ . The Overflow Water (OW)
754 properties are a mixture of aW and SW determined by entrainment Φ . The entrainment Φ
755 depends on the density difference $\Delta\rho$ between aW and SW from (17). 45

756 **Fig. 4.** Results for experiment 1, with parameters appropriate for the Arctic (Fram Strait and Barents
757 Sea Opening, BSO). The upper panel shows temperature/salinity properties T_i, S_i for AW
758 ($i = 1$), SW ($i = s$), aW ($i = a$), OW ($i = 3$), and PW ($i = 2$). The curved black contours are
759 the density anomaly $\rho(T, S) - 1000\text{kgm}^{-3}$. The thick black line is the freezing temperature.
760 The brown and green patches show the range of possible OW properties from the theories in
761 supplement sections S5 and S6, respectively. The left (right) column of panels show mass,
762 salt, and heat fluxes crossing section A (B) in Fig. 2. The individual terms in (S1) and
763 (S2) are shown with the horizontal bars. The blue error bars indicate the range of possible
764 solutions (see text). This solution is entrainment dominated with $\Phi \approx 0.94$, warm OW, and
765 a weak shelf circulation. 46

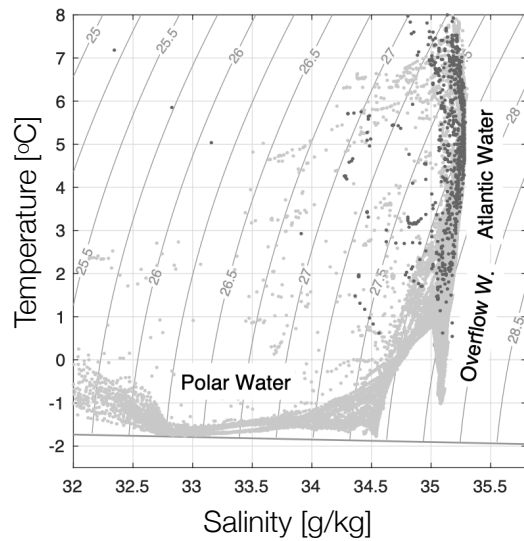
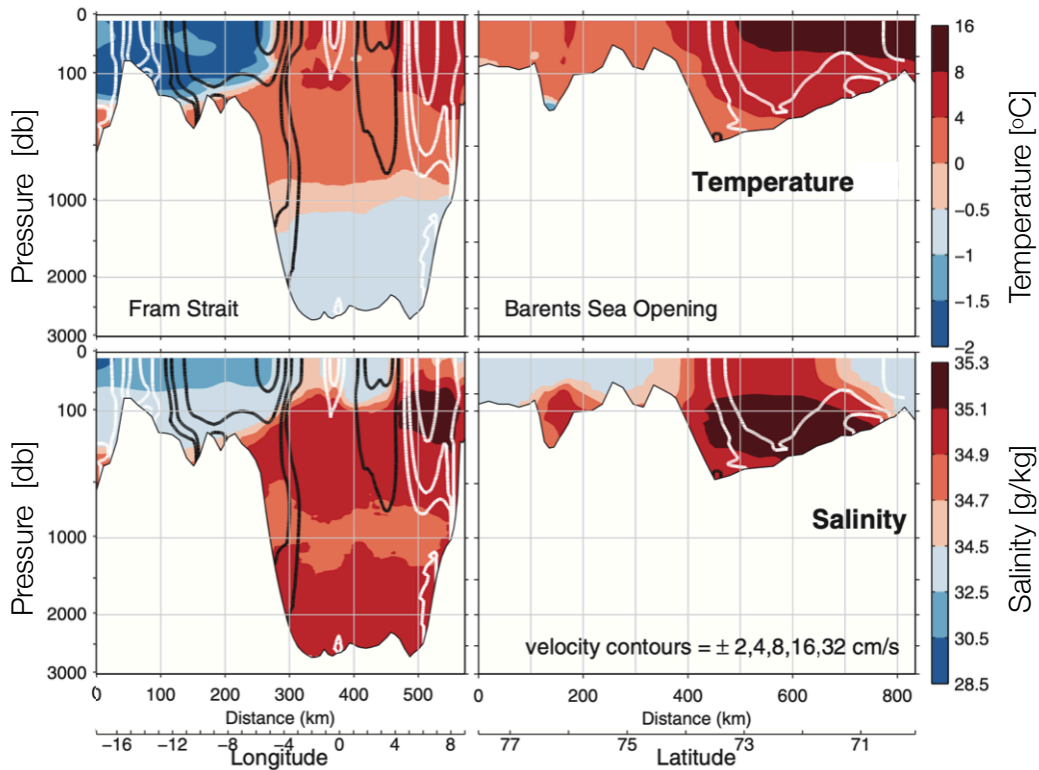
766 **Fig. 5.** As Fig. 4, except for experiment 2. This solution has similar mass and salt fluxes to experiment
767 1 shown in Fig. 4, but weak entrainment ($\Phi \approx 0.13$), strong shelf circulation, and cold OW.
768 The total ocean heat loss flux, Q is 33% times larger than for experiment 1. Notice the heat
769 flux abscissa limits differ from Fig. 4. 47

770 **Fig. 6.** Results for experiment 3 for the Arctic. The top panel shows the normalized volume fluxes
771 U_2, U_3 , and U_i . The middle panel shows the OW properties T_3 and S_3 . The bottom panel
772 shows the entrainment Φ . In each case, the abscissa is the normalized ocean heat loss flux
773 Q . The solid and dashed vertical lines indicate experiments 1 and 2, shown in Figs. 4 and 5,
774 respectively. The hatched regions indicate no solutions are possible because $U_2 \not\leq 0$; see text
775 for details. 48

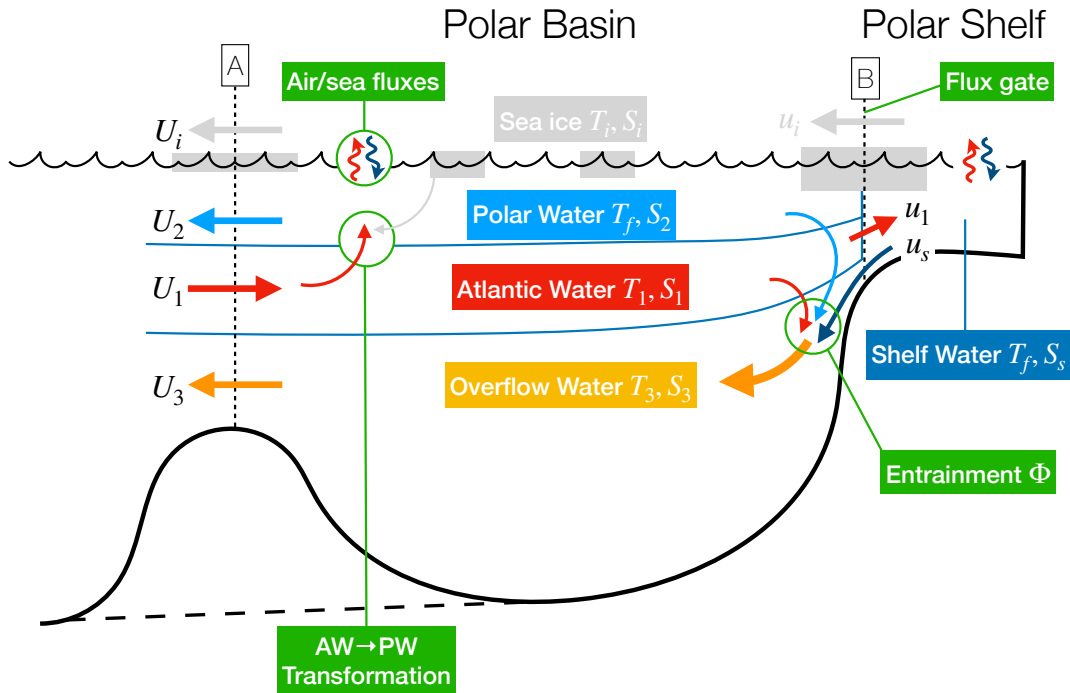
776 **Fig. 7.** Schematic of the tradeoff between entrainment Φ and shelf salinity S_s for fixed OW flux.
777 Strong (weak) entrainment implies weak (strong) shelf circulation u_s from (21). Results
778 from experiments 1 and 2, including the range of possible solutions, are shown. The theory
779 curve is from (28). 49

780 **Fig. 8.** Results for experiment 4 for the Arctic. Normalized distributions of U_2, U_3 , and U_i against
781 the forcing parameter $\mathcal{N}^* = L'\mathcal{F} + (1 - S_i/S_1)Q + c_p\rho_0(S_i/S_1 - 1)T_1U_1$ for many solutions
782 with different parameters $\{\mathcal{F}, Q, U_1, T_1, S_1\}$ (see Table 2). In each case, the distribution is
783 taken of the solutions with entrainment closest to the mean entrainment, like the bars in

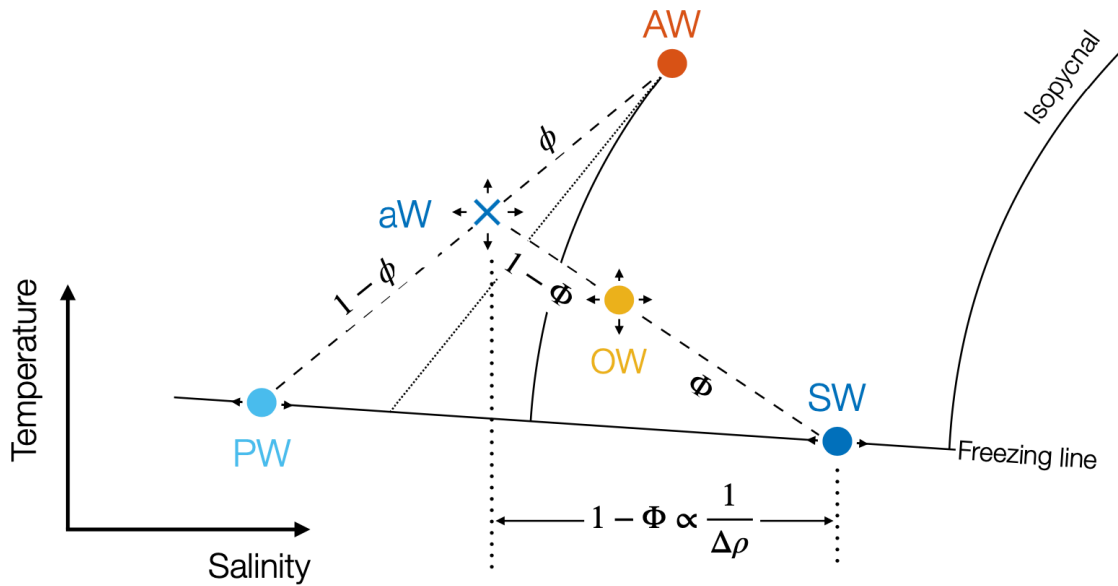
784	Fig. 4. The solid and dashed vertical lines indicate experiments 1 and 2, shown in Figs. 4 and	
785	5, respectively. The white curves show the results from experiment 3, as in Fig. 6, which are	
786	a subset of the results from experiment 4. There are 525199 valid solutions in experiment 4.	50
787	Fig. 9. Parametric locations of heat and salt crises, and OW emergency. The abscissa plots normal-	
788	ized forcing parameter $\mathcal{N}^* = L'\mathcal{F} + (1 - S_i/S_1)Q + c_p\rho_0(S_i/S_1 - 1)T_1U_1$ from the numerical	
789	solutions to experiments 4. The ordinate plots the corresponding values of \mathcal{N}^* from the theory	
790	in supplement section S4. The black diagonal line indicates perfect agreement between	
791	theory and the numerical results.	51
792	Fig. 10. As Fig. 6, except for experiment 5, illustrating the approach to the entrainment emergency.	52
793	Fig. 11. As Fig. 4, except for experiment 6 for the Antarctic.	53
794	Fig. 12. Schematics of the four main solution modes: (a) Heat crisis for small Q (like experiment	
795	1), (b) OW emergency for intermediate Q (like experiment 6 and the middle of experiment	
796	3), (c) Salt crisis for large Q (like experiment 2), and (d) Entrainment emergency for fresh	
797	PW and/or aW (like the small PW salinity end of experiment 5). These main solutions are	
798	determined by the forcing, indicated by the ocean heat loss flux Q (Figs. 6 and 8), and by the	
799	aW salinity (Fig. 10). See also supplement Fig. S1.	54



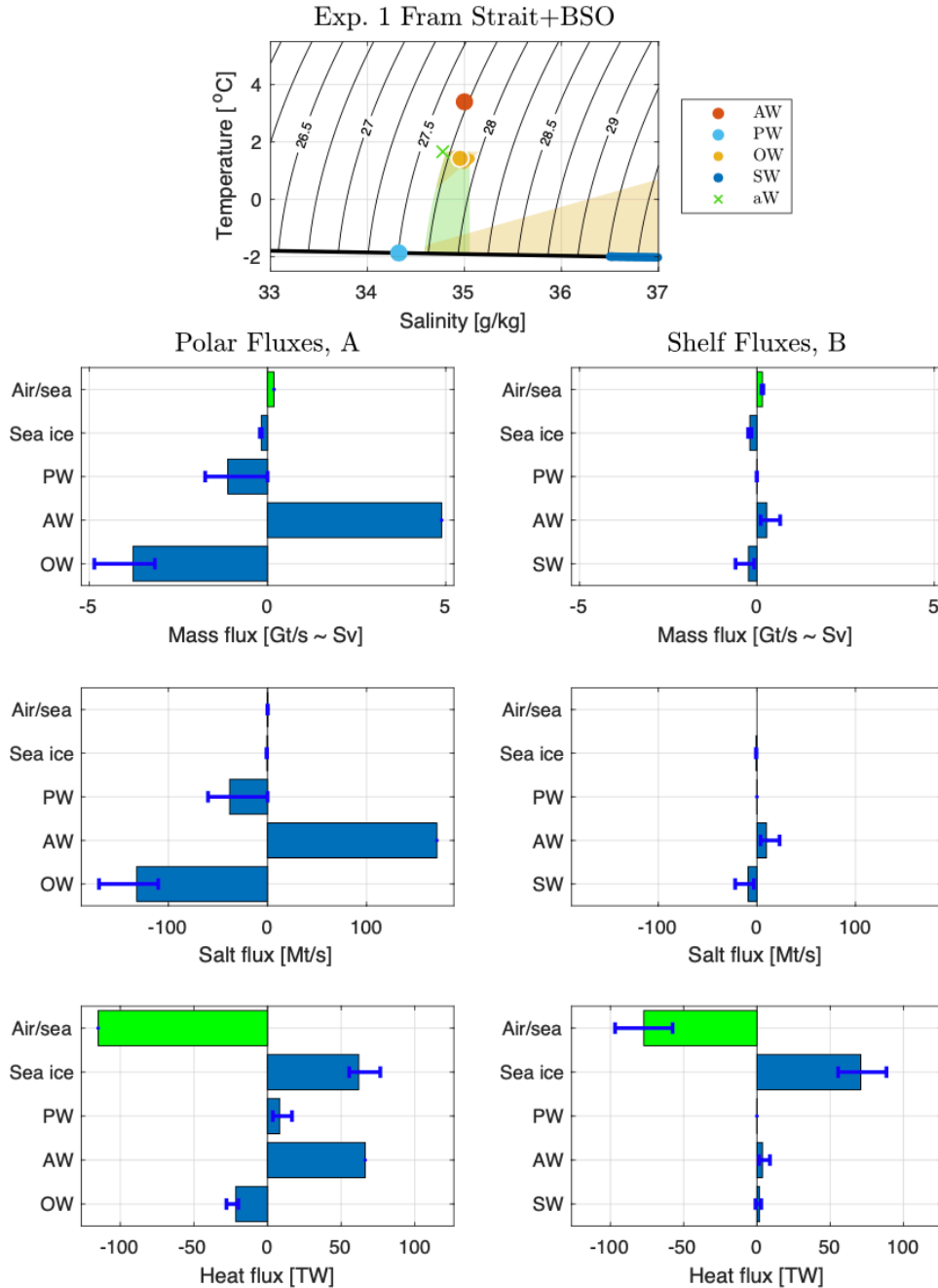
800 FIG. 1. Upper two panels: Observations of temperature, salinity and normal geostrophic current across the
 801 Fram Strait and Barents Sea Opening. Modified from Klinger and Haine (2019) and based on results from
 802 Tsubouchi et al. (2012). Lower panel: Temperature and salinity data from Fram Strait in August 2002 (light
 803 gray) and from the Barents Sea Opening in August 2017 (dark gray; from the World Ocean Database, Boyer et al.
 804 2018).



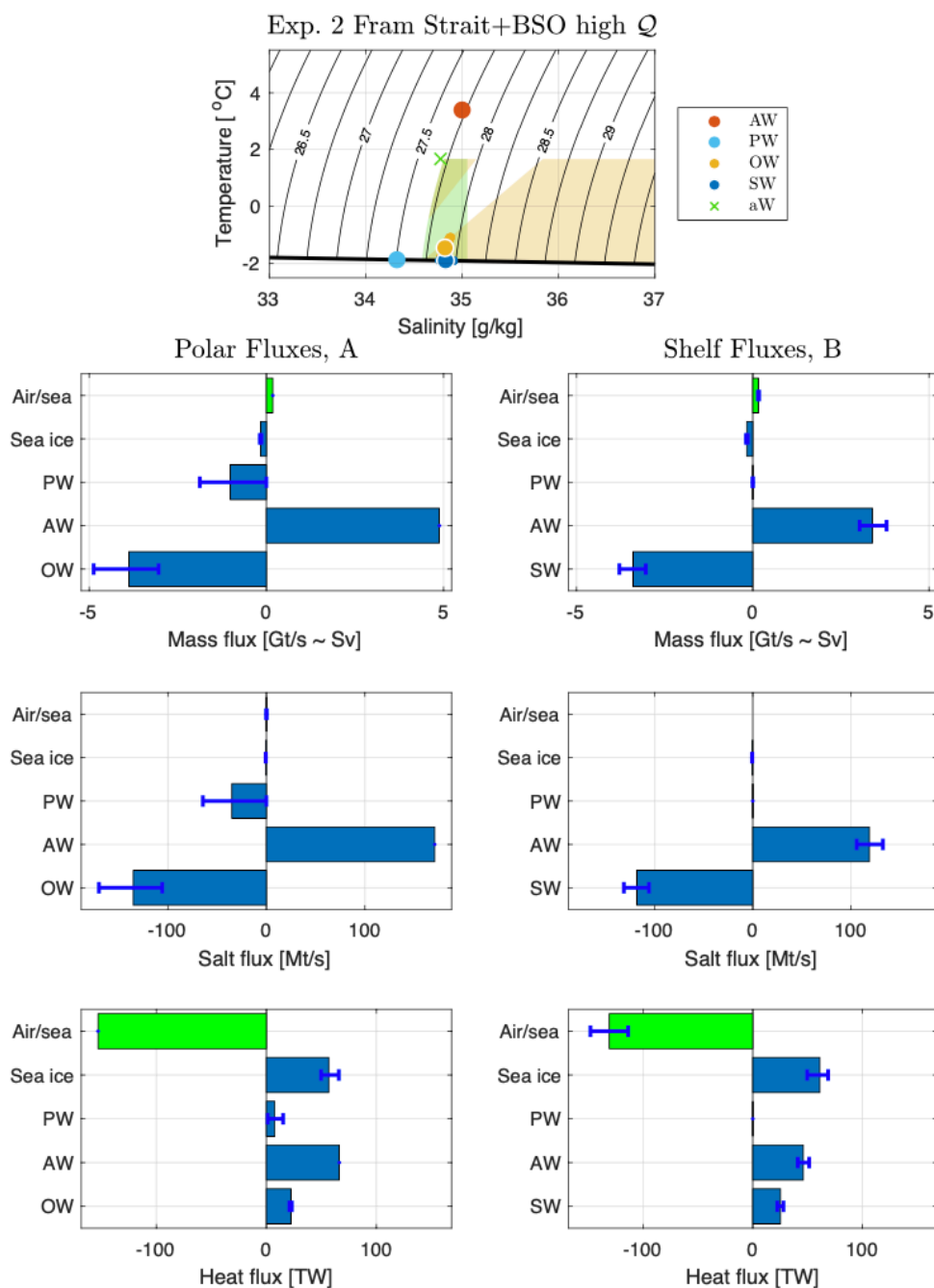
805 FIG. 2. Schematic of the conceptual polar overturning model. The sign convention is that positive volume
 806 fluxes are towards the right. For plausible solutions $\{U_2, U_3, U_i, u_s, u_i\} < 0$ and $u_1 > 0$, as the arrows show. The
 807 bathymetric bump at section A (nominally, the Fram Strait and Barents Sea Opening) is for illustrative purposes:
 808 the dashed line represents the Antarctic case. Table 1 defines the symbols.



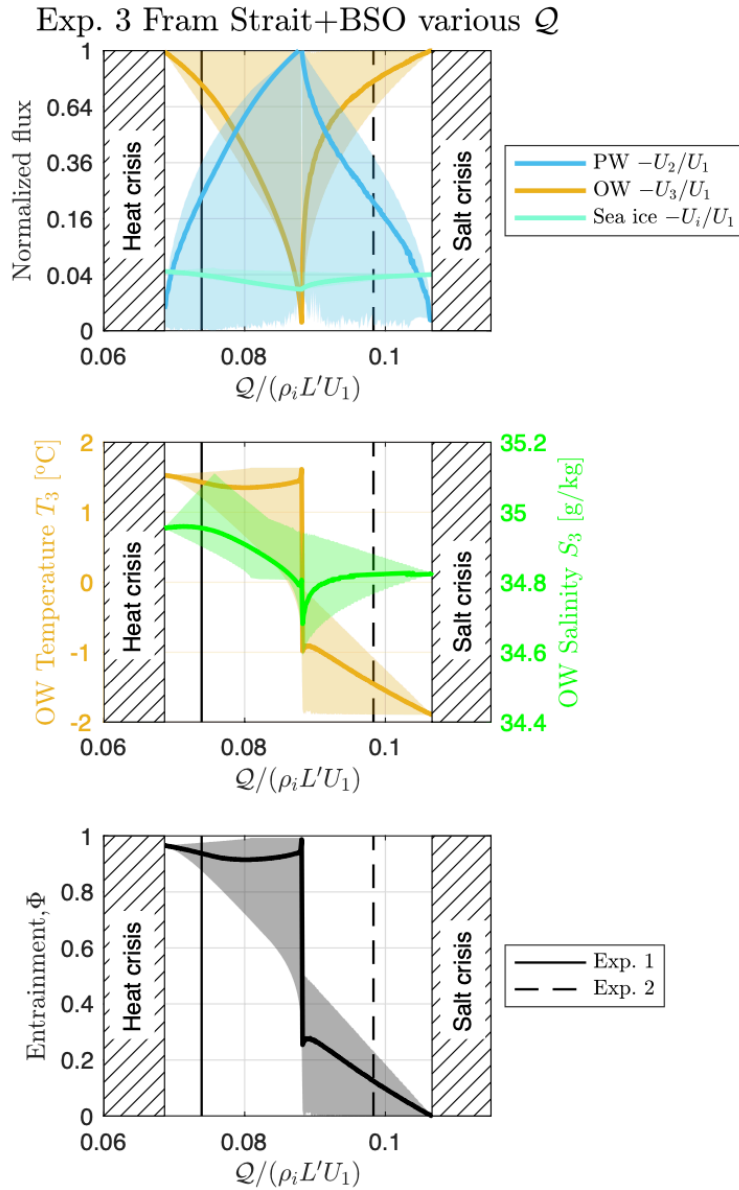
809 FIG. 3. Schematic of the processes affecting OW properties. The Atlantic Water (AW) properties are specified.
 810 The Polar Water (PW) properties are freezing temperature and salinity less than the maximum value given by
 811 the dotted line tangent to the AW isopycnal. The ambient Water (aW) properties are a mixture of PW and AW
 812 determined by ϕ . The Overflow Water (OW) properties are a mixture of aW and SW determined by entrainment
 813 Φ . The entrainment Φ depends on the density difference $\Delta\rho$ between aW and SW from (17).



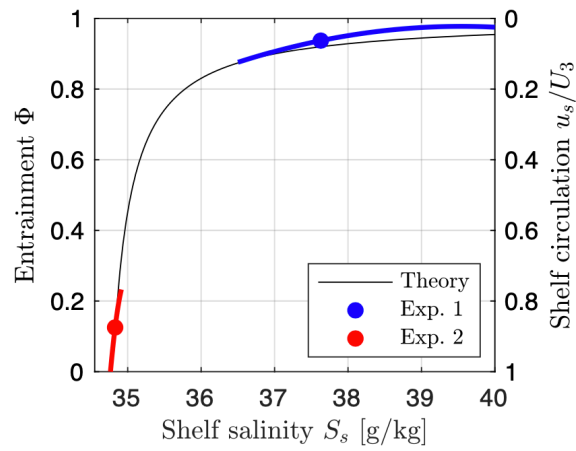
814 FIG. 4. Results for experiment 1, with parameters appropriate for the Arctic (Fram Strait and Barents Sea
 815 Opening, BSO). The upper panel shows temperature/salinity properties T_i, S_i for AW ($i = 1$), SW ($i = s$), aW
 816 ($i = a$), OW ($i = 3$), and PW ($i = 2$). The curved black contours are the density anomaly $\rho(T, S) - 1000\text{kgm}^{-3}$.
 817 The thick black line is the freezing temperature. The brown and green patches show the range of possible OW
 818 properties from the theories in supplement sections S5 and S6, respectively. The left (right) column of panels
 819 show mass, salt, and heat fluxes crossing section A (B) in Fig. 2. The individual terms in (S1) and (S2) are shown
 820 with the horizontal bars. The blue error bars indicate the range of possible solutions (see text). This solution is
 821 entrainment dominated with $\Phi \approx 0.94$, warm OW, and a weak shelf circulation.



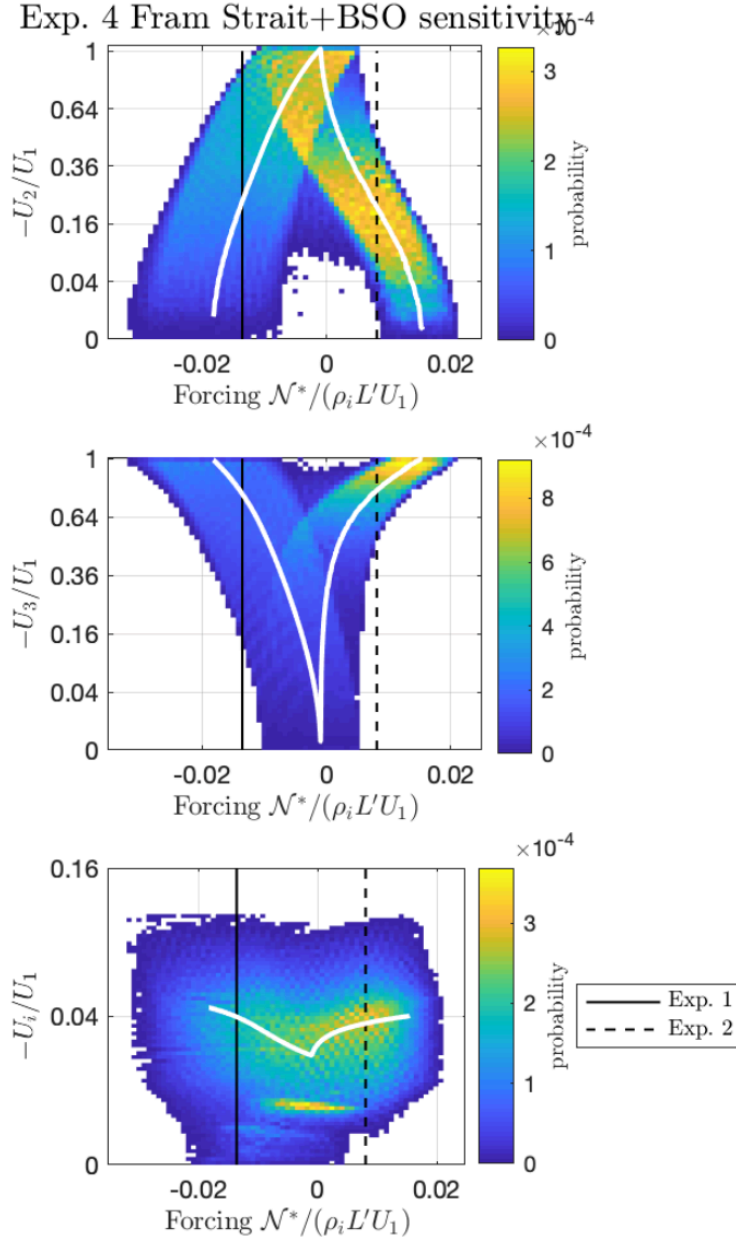
822 FIG. 5. As Fig. 4, except for experiment 2. This solution has similar mass and salt fluxes to experiment 1
 823 shown in Fig. 4, but weak entrainment ($\Phi \approx 0.13$), strong shelf circulation, and cold OW. The total ocean heat
 824 loss flux, Q is 33% times larger than for experiment 1. Notice the heat flux abscissa limits differ from Fig. 4.



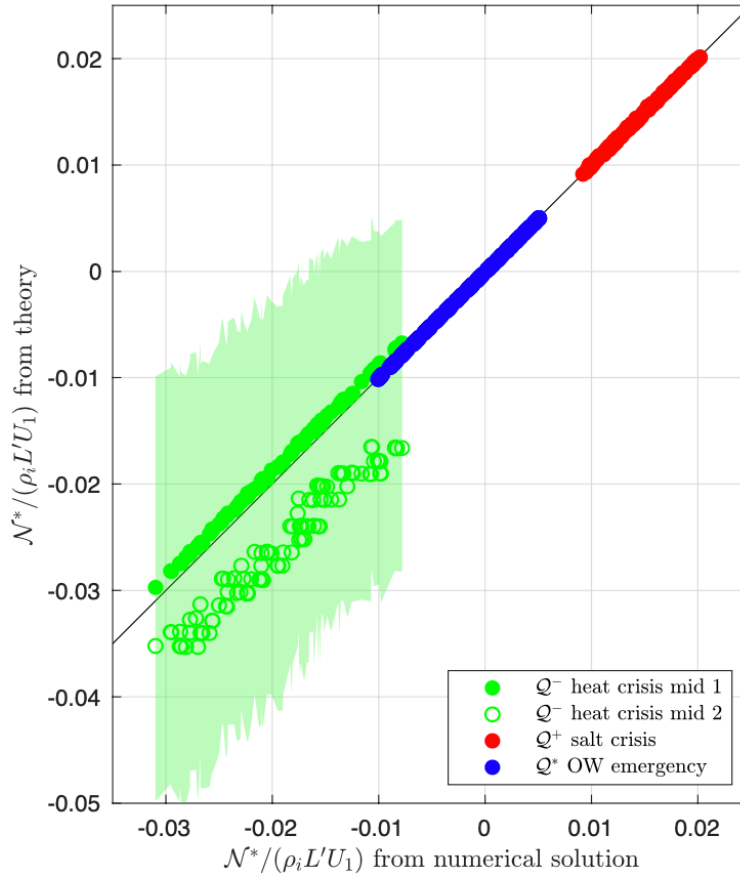
825 FIG. 6. Results for experiment 3 for the Arctic. The top panel shows the normalized volume fluxes $U_2, U_3,$
 826 and U_i . The middle panel shows the OW properties T_3 and S_3 . The bottom panel shows the entrainment Φ . In
 827 each case, the abscissa is the normalized ocean heat loss flux Q . The solid and dashed vertical lines indicate
 828 experiments 1 and 2, shown in Figs. 4 and 5, respectively. The hatched regions indicate no solutions are possible
 829 because $U_2 \neq 0$; see text for details.



830 FIG. 7. Schematic of the tradeoff between entrainment Φ and shelf salinity S_s for fixed OW flux. Strong (weak)
 831 entrainment implies weak (strong) shelf circulation u_s from (21). Results from experiments 1 and 2, including
 832 the range of possible solutions, are shown. The theory curve is from (28).



833 FIG. 8. Results for experiment 4 for the Arctic. Normalized distributions of U_2, U_3 , and U_i against the
 834 forcing parameter $\mathcal{N}^* = L'\mathcal{F} + (1 - S_i/S_1)\mathcal{Q} + c_p \rho_0 (S_i/S_1 - 1)T_1 U_1$ for many solutions with different parameters
 835 $\{\mathcal{F}, \mathcal{Q}, U_1, T_1, S_1\}$ (see Table 2). In each case, the distribution is taken of the solutions with entrainment closest to
 836 the mean entrainment, like the bars in Fig. 4. The solid and dashed vertical lines indicate experiments 1 and 2,
 837 shown in Figs. 4 and 5, respectively. The white curves show the results from experiment 3, as in Fig. 6, which
 838 are a subset of the results from experiment 4. There are 525199 valid solutions in experiment 4.



839 FIG. 9. Parametric locations of heat and salt crises, and OW emergency. The abscissa plots normalized forcing
 840 parameter $N^* = L' \mathcal{F} + (1 - S_i/S_1) Q + c_p \rho_0 (S_i/S_1 - 1) T_1 U_1$ from the numerical solutions to experiments 4. The
 841 ordinate plots the corresponding values of N^* from the theory in supplement section S4. The black diagonal
 842 line indicates perfect agreement between theory and the numerical results.

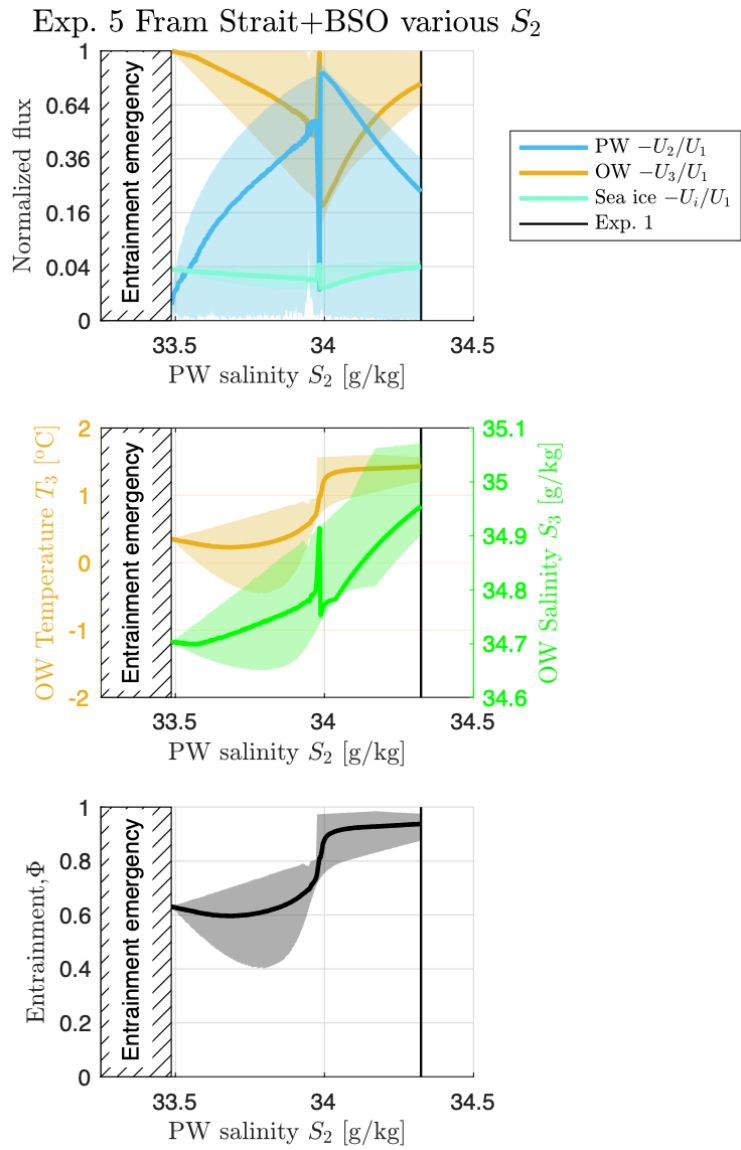


FIG. 10. As Fig. 6, except for experiment 5, illustrating the approach to the entrainment emergency.

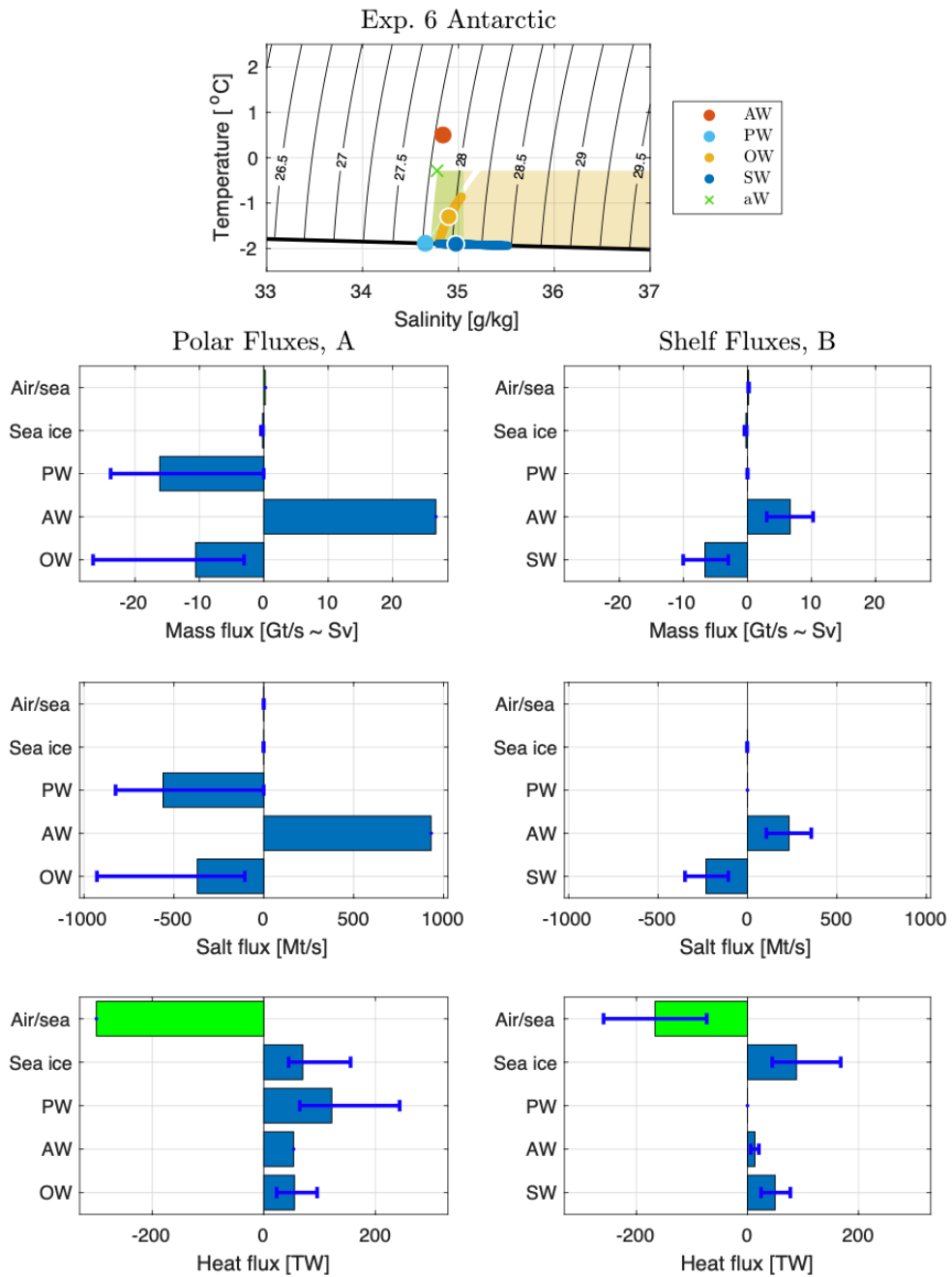
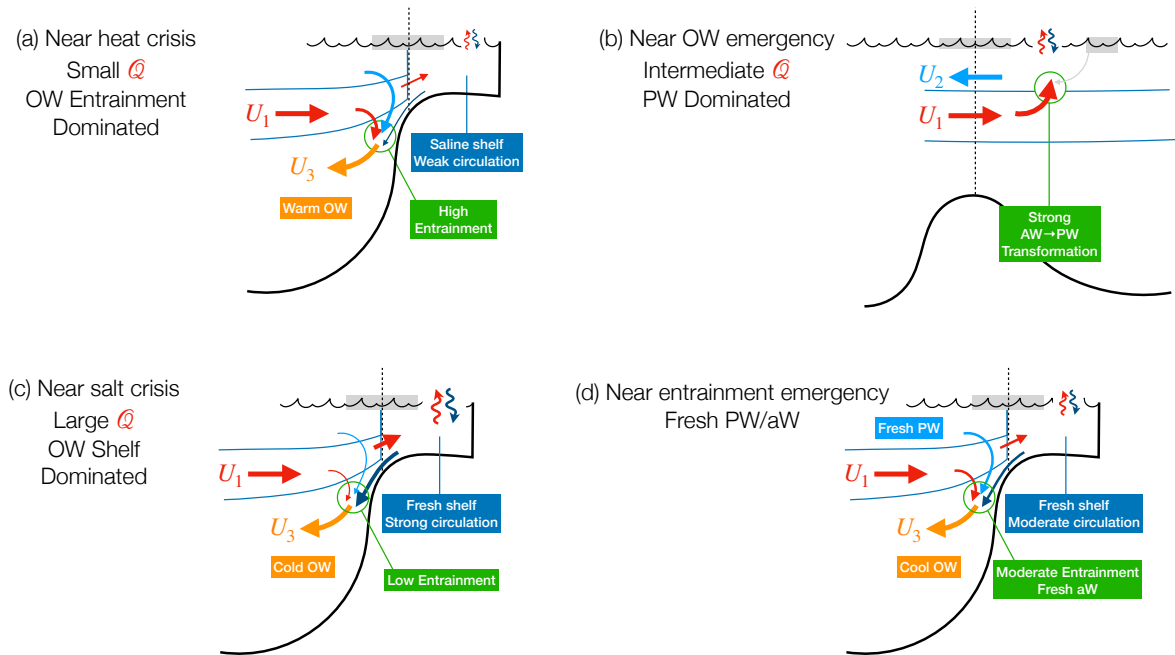


FIG. 11. As Fig. 4, except for experiment 6 for the Antarctic.



843 FIG. 12. Schematics of the four main solution modes: (a) Heat crisis for small Q (like experiment 1), (b)
 844 OW emergency for intermediate Q (like experiment 6 and the middle of experiment 3), (c) Salt crisis for large
 845 Q (like experiment 2), and (d) Entrainment emergency for fresh PW and/or aW (like the small PW salinity end
 846 of experiment 5). These main solutions are determined by the forcing, indicated by the ocean heat loss flux Q
 847 (Figs. 6 and 8), and by the aW salinity (Fig. 10). See also supplement Fig. S1.